Atmos. Chem. Phys. Discuss., 11, 11311–11378, 2011
www.atmos-chem-phys-discuss.net/11/11311/2011/
doi:10.5194/acpd-11-11311-2011

Atmospheric Chemistry and Physics Discussions

Observation and modelling of OH and HO_2 concentrations in the Pearl River Delta 2006: a missing OH source in a VOC rich atmosphere

K. D. Lu[1,2], F. Rohrer[2], F. Holland[2], H. Fuchs[2], B. Bohn[2], T. Brauers[2], C. C. Chang[3], R. Häseler[2], M. Hu[1], K. Kita[4], Y. Kondo[5], X. Li[1,2], S. R. Lou[2,6], S. Nehr[2], M. Shao[1], L. M. Zeng[1], A. Wahner[2], Y. H. Zhang[1], and A. Hofzumahaus[2]

[1]College of Environmental Sciences and Engineering, Peking University, Beijing, China
[2]Institut für Energie und Klimaforschung: Troposphäre, Forschungszentrum Jülich, Jülich, Germany
[3]Research Center for Environmental Changes, Academic Sinica, Taipei, China
[4]Faculty of Science, Ibaraki University, Ibaraki, Japan
[5]University of Tokyo, Research Center for Advanced Science and Technology, Tokyo, Japan
[6]School of Environmental Science and Technology, Shanghai Jiao Tong University, Shanghai, China

Received: 28 March 2011 – Accepted: 31 March 2011 – Published: 12 April 2011

Correspondence to: A. Hofzumahaus (a.hofzumahaus@fz-juelich.de) and
Y. H. Zhang (yhzhang@pku.edu.cn)

Published by Copernicus Publications on behalf of the European Geosciences Union.

Abstract

Ambient OH and HO_2 concentrations were measured by laser induced fluorescence (LIF) during the PRIDE-PRD2006 (Program of Regional Integrated Experiments of Air Quality over the Pearl River Delta, 2006) campaign at a rural site downwind of the megacity of Guangzhou in Southern China. The observed OH concentrations reached daily peak values of $(15–26) \times 10^6\,cm^{-3}$ which are among the highest values so far reported for urban and suburban areas. The observed OH shows a consistent high correlation with $j(O^1D)$ over a broad range of NO_x conditions. The correlation cannot be reproduced by model simulations, indicating that OH stabilizing processes are missing in current models. The observed OH exhibited a weak dependence on NO_x in contrast to model predictions. While modelled and measured OH agree well at NO mixing ratios above 1 ppb, a continuously increasing underprediction of the observed OH is found towards lower NO concentrations, reaching a factor of 8 at 0.02 ppb NO. A dependence of the modelled-to-measured OH ratio on isoprene cannot be concluded from the PRD data. However, the magnitude of the ratio fits into the isoprene dependent trend that was reported from other campaigns in forested regions. Hofzumahaus et al. (2009) proposed an unknown OH recycling process without NO, in order to explain the high OH levels at PRD in the presence of high VOC reactivity and low NO. Taking a recently discovered interference in the LIF measurement of HO_2 into account, the need for an additional $HO_2 \rightarrow OH$ recycling process persists, but the required source strength may be up to 20% larger than previously determined. Recently postulated isoprene mechanisms by Lelieveld et al. (2008) and Peeters and Müller (2010) lead to significant enhancements of OH expected for PRD, but an underprediction of the observed OH by a factor of two remains at low NO (0.1–0.2 ppb). If the photolysis of hydroperoxy aldehydes from isoprene is as efficient as proposed by Peeters and Müller (2010), the corresponding OH formation at PRD would be more important than the primary OH production from ozone and HONO. While the new isoprene mechanisms need to be confirmed by laboratory experiments, there is probably need for other, so

far unidentified chemical processes to explain entirely the high OH levels observed in Southern China.

1 Introduction

Hydroxyl (OH) and peroxy (HO_2, RO_2) radicals play an essential role in atmospheric chemistry on local to global scales (e.g., Brasseur et al., 2003; Monks et al., 2009). Reactions with the most important atmospheric oxidant, OH, initiate the chemical breakdown of tropospheric trace gases such as CO, SO_2, NO_2, CH_4 and other volatile organic compounds (VOCs). Many of these reactions produce HO_2 and RO_2, which are key intermediates in the formation of secondary, atmospheric pollutants (Finlayson-Pitts and Pitts Jr., 2000). Reactions (R1)–(R4) represent examples of HO_2 and RO_2 forming reactions:

$$\mathrm{CO + OH \rightarrow H + CO_2} \tag{R1}$$

$$\mathrm{H + O_2 + M \rightarrow HO_2 + M} \qquad \mathrm{(M = N_2, O_2)} \tag{R2}$$

$$\mathrm{RH + OH \rightarrow R + H_2O} \qquad \mathrm{(R = organic\ group)} \tag{R3}$$

$$\mathrm{R + O_2 + M \rightarrow RO_2 + M}. \tag{R4}$$

Reactions of peroxy radicals with NO constitute the exclusive pathway for tropospheric ozone formation,

$$\mathrm{RO_2 + NO \rightarrow RO + NO_2} \tag{R5}$$

$$\mathrm{RO + O_2 \rightarrow R'O + HO_2} \tag{R6}$$

$$\mathrm{HO_2 + NO \rightarrow OH + NO_2} \tag{R7}$$

$$\mathrm{NO_2} + h\nu(\lambda < 420\,\mathrm{nm}) \rightarrow \mathrm{NO + O} \tag{R8}$$

$$\mathrm{O + O_2 + M \rightarrow O_3 + M} \tag{R9}$$

and recombination reactions of peroxy radicals represent a source of peroxides (H_2O_2, ROOH).

$$HO_2 + HO_2 \rightarrow H_2O_2 + O_2 \tag{R10}$$

$$RO_2 + HO_2 \rightarrow ROOH + O_2. \tag{R11}$$

Oxy radicals, RO, produced by Reaction (R5), are generally converted to oxygenated VOCs (OVOCs), either by fast reaction with O_2 yielding carbonyl compounds, R′O (Reaction R6), or by unimolecular decomposition and isomerization reactions (Atkinson, 1997). OVOCs are currently receiving growing attention in atmospheric chemistry. Firstly, they may contribute significantly, sometimes 50% and more to the organic reactivity in various tropospheric environments, thereby affecting the atmospheric lifetime of OH (Lou et al., 2010; Mao et al., 2010; Shao et al., 2009; Steiner et al., 2008; Emmerson et al., 2007; Yoshino et al., 2006; Lewis et al., 2005). Secondly, photolysis of OVOCs can be a significant source of radicals at urban conditions (Emmerson et al., 2007; Kanaya et al., 2007b; Volkamer et al., 2007; Dusanter et al., 2009). Thirdly, OVOCs are precursors of secondary organic aerosols (SOA) which play a distinct role for air quality and climate (e.g., Hallquist et al., 2009; Kanakidou et al., 2005).

The atmospheric abundance of OH and HO_2, collectively called HO_X, depends critically on primary production processes with contributions by photolysis of ozone,

$$O_3 + h\nu(\lambda < 340\,\mathrm{nm}) \rightarrow O(^1D) + O_2(^1\Delta,^3\Sigma) \tag{R12}$$

$$O(^1D) + H_2O \rightarrow OH + OH \tag{R13}$$

photolysis of nitrous acid and OVOCs, and O_3-alkene reactions (Fig. 1). Ensuing chain reactions (Reaction R1–R7, indicated by red arrows in Fig. 1) oxidize CO, VOCs and NO, but also interconvert RO_X radicals ($= OH + HO_2 + RO_2$). Radical recycling by Reactions (R5)–(R7) is of particular relevance, as it constitutes a secondary source of OH which significantly enhances the oxidation efficiency of the troposphere (e.g., Ehhalt, 1999). Radical recombination reactions (e.g., Reactions R10, R11, R14, R15), however, cause chain termination and suppress the concentrations of OH, HO_2 and RO_2

radicals.

$$OH + NO_2 + M \rightarrow HNO_3 + M \quad \text{(R14)}$$

$$RO_2 + NO + M \rightarrow RONO_2 + M \quad \text{(R15)}$$

Highly sensitive instruments for in-situ measurement of HO_X became available in the 1990s (Crosley, 1995) and have been employed in an increasing number of field experiments to test atmospheric chemical mechanisms over a broad range of tropospheric conditions. Early studies were carried out mostly in clean (polar, marine) and moderately polluted (rural) regions (Heard and Pilling, 2003), whereas many recent investigations were focussed on environments with high loads of reactive trace gases (Monks et al., 2009). These include polluted cities and their urban-influenced surroundings, as well as forests with high concentrations of biogenic VOCs. Most urban studies have shown reasonable agreement between modelled and measured OH within a factor of two when VOCs and NO_X were abundant (e.g., Kanaya et al., 2007b; Shirley et al., 2006; Mihelcic et al., 2003). However, current models tend to underpredict the observed OH by up to an order of magnitude at low NO_X, when isoprene reaches mixing ratios of several ppb at the same time. This trend has been clearly identified in forested regions, such as in North America (Tan et al., 2001; Ren et al., 2008), over the Amazonian rainforest (Lelieveld et al., 2008) and the tropical forest of Borneo (Pugh et al., 2010; Whalley et al., 2011). The observations suggest that as-yet-unknown recycling reactions of peroxy radicals constitute a significant OH source, when NO mixing ratios become small. This hypothesis is consistent with a budget analysis of HO_X in isoprene-containing urban air near Nashville by Thornton et al. (2002), who supposed that self reactions of peroxy radicals possibly recycle OH, rather than acting as an HO_X sink (Reaction R11).

The above findings from urban and forest studies are in agreement with our investigation in Southern China (Hofzumahaus et al., 2009). In summer 2006, we performed a field campaign in the densely populated Pearl River Delta (PRD), close to the megacity of Guangzhou in Guandong province, where atmospheric conditions were strongly influenced by both urban and biogenic emissions. Since many years, this subtropical region is experiencing severe air pollution resulting from a fast growing econonomy and increasing urbanization (Chan and Yao, 2008; Zhang et al., 2008). At a rural site downwind of Guangzhou, we performed the ground-based field campaign PRIDE-PRD2006 (Program of Regional Integrated Experiments of Air Quality over the Pearl River Delta, 2006), in order to study the photochemical processing of atmospheric urban pollutants (Zhang et al., 2011, 2011). During the intensive campaign, trace gases, photolysis frequencies, aerosols, and meteorological parameters were measured. The measurements included OH and HO_2, as well as the total OH reactivity, k_{OH}, which is equivalent to the reciprocal atmospheric OH lifetime (Lou et al., 2010).

On most days, the local atmosphere changed from an urban-type composition with high concentrations of anthropogenic VOCs and NO_X in the morning to an atmosphere with relatively low NO (0.1–0.2 ppb) and a significant biogenic contribution (≈ 40%) of isoprene and its oxidation products to k_{OH} in the afternoon (Lou et al., 2010). The field campaign data were used to evaluate the OH budget by comparing the experimental OH loss rate, $k_{OH} \times [OH]$, with the total OH production rate, P'_{OH}, of the known primary (e.g., Reaction R13) and secondary OH production (Reaction R7) processes (Hofzumahaus et al., 2009). The OH loss rate was found to be balanced by P'_{OH} in the morning, when HO_2 was efficiently recycled to OH by reaction with NO (1–20 ppb). However, P'_{OH} was significantly smaller (by about a factor ≈ 3 at noon) than $k_{OH} \times [OH]$, when NO decreased to values below 1 ppb around and past noon, indicating a missing OH source.

The OH budget analysis was consistent with a comparison of model and measurement results for OH and k_{OH}. For k_{OH}, agreement of measured and modelled values was obtained within 20% during the whole daytime, suggesting that the total reactivity of OH reactants was well determined at high and low NO_X conditions (Lou et al., 2010). In case of OH, modelled and measured concentrations were in agreement at high NO_X in the morning, but a significant underprediction of measured OH by a factor 3–5 was found in the afternoon at low NO_X (Hofzumahaus et al., 2009). The model could be matched to the afternoon OH observations by assuming additional NO-independent recycling of OH from peroxy radicals, without impairing the good agreement between model and measurement results in the morning hours. The interesting question is, whether the missing OH sources postulated for tropical forests, North American forests, and the densely-populated PRD region are mechanistically the same.

Butler et al. (2008) and Kubistin et al. (2010) introduced an artificial reaction of isoprene hydroxyperoxy radicals (ISOP) with HO_2 ($ISOP + HO_2 \rightarrow n OH$) into global and box models, respectively, to simulate the assumed additional OH recycling over the Amazonian rainforest. For best fit to the OH observations, OH yields of $n = 2$ and $n = 3.2$ were required in the respective models. In order to describe the measured data of OH and HO_2 at PRD, Hofzumahaus et al. (2009) implemented two hypothetical reactions ($RO_2 + X \rightarrow HO_2$ and $HO_2 + X \rightarrow OH$, both of the same rate as for the corresponding NO reactions) into a box model. An NO equivalent of 0.8 ppb was assumed for X to match the mean diurnal profiles of both HO_X species.

Recent model studies have attempted to identify the actual reaction mechanisms underlying the non-classical (without NO) OH recycling in forested regions. OH regenerating reactions of HO_2 with acyl peroxy and β-keto peroxy radicals, known from various laboratory studies (Jenkin et al., 2010, 2007; Dillon and Crowley, 2008; Hasson et al., 2004), were found to increase modelled OH by at most 7% above tropical rainforests (Peeters and Müller, 2010; Stavrakou et al., 2010; Archibald et al., 2010; Pugh et al., 2010). In addition, the OH-neutral oxidation of isoprene hydroperoxides to dihydroxy epoxides, experimentally studied by Paulot et al. (2009), has the potential to further increase the modelled OH concentration by up to 25% in the tropics, depending on the specific isoprene degradation mechanism being used (Stavrakou et al., 2010; Archibald et al., 2010). However, even together the above processes are not sufficient to explain the factor-of-10 discrepancy between modelled and observed OH above the Amazonian rainforest.

Based on *ab initio* calculations, Peeters et al. (2009) and Peeters and Müller (2010) have postulated a new isoprene degradation mechanism (Leuven Isoprene

Title Page
Abstract Introduction
Conclusions References
Tables Figures
◀| |▶
◀ ▶
Back Close
Full Screen / Esc
Printer-friendly Version
Interactive Discussion

Mechanism, LIM0) which recycles HO_X with high efficiency at low NO. The new mechanism proposes a fast interconversion of isoprene hydroxyperoxy radical isomers, some of which undergo fast 1,6-H shift, followed by reaction with O_2. This predominating reaction path is expected to form HO_2 and hydroperoxy aldehydes (HPALDs). The HPALDs are assumed to undergo photodissociation at a high photolysis rate, leading to a net formation of one HO_2 and up to three OH radicals. The implementation of the LIM0 mechanism increases the modelled OH concentrations for the conditions over the Amazonian rainforest by up to a factor of four, showing potential to explain the non-classical OH recycling in regions with high isoprene emissions (Stavrakou et al., 2010; Archibald et al., 2010).

In the present work, we investigate whether the newly proposed recycling mechanisms can explain the high OH levels at PRD, where NO concentrations span a broad range (0.02–10 ppb) and where anthropogenic VOCs are present besides isoprene. First, we report experimental details of the measurements of HO_X during the PRIDE-PRD2006 campaign and demonstrate the stabilizing effect of the unknown OH source on the observed OH concentration as a function of the ozone photolysis frequency, $j(O^1D)$, and NO_X. We test different recycling mechanisms to investigate their impact on atmospheric OH and HO_2 for the conditions at PRD. The analysis is complicated by a recently discovered interference in our HO_2 measurements, which are significantly biased by the detection of specific organic peroxy radicals, such as isoprene hydroxyperoxy radicals (Nehr et al., 2011; Fuchs et al., 2011). The results reported by Hofzumahaus et al. (2009) are revised, accordingly.

2 Methodology

2.1 Measurement site

The measurements presented in this paper took place alongside a drinking water reservoir in a recreation area called Guangzhou Backgarden about 60 km northwest of downtown Guangzhou on 3–30 July 2006. Backgarden is located in a slightly mountainous area at 23.487° N, 113.034° E and is surrounded by farmland, which is mainly covered by tropical shrubs and economic crops like lichees and peanuts. During the intensive campaign period, due to Asian monsoon, the dominant wind direction was south to south east, making Backgarden a receptor site for the outflow of urban emissions from Guangzhou. However, local wind speeds were generally low (often less than 2 m s^{-1}), which is typical for inland PRD during summer season and favors accumulation of air pollutants (Chan and Yao, 2008). During the campaign, the weather was characterized by high humidity with absolute water-vapor mixing ratios of 2.5–4% and high temperatures of about 28–36 °C.

Besides HO_X (see next section), a comprehensive set of trace gases was measured during the campaign. Table 1 gives an overview of the measured species which are relevant for this paper and specifies the measurement techniques and their performance. Further instrumental details can be found in Lou et al. (2010). The C_3–C_{12} VOCs, measured by online gas chromatography (GC), are specified in Table 2. They include alkanes, alkenes, aromatics, and isoprene. No in-situ OVOCs measurements were available; but on some days, the averaged HCHO and glyoxal concentrations for certain air masses spanning several kilometers were retrieved by MAX-DOAS (Li et al., 2010). Most trace gases were sampled at 10 m above ground on top of a building. HO_X, k_{OH}, HONO and meteorological data were measured nearby (30 m distance) at 7 m height on top of two stacked sea containers. On the containers, the photolysis frequencies $j(O^1D)$ for Reaction (R12) and $j(NO_2)$ for Reaction (R8) were measured by calibrated filterradiometers. On the nearby building, $j(O^1D)$, $j(NO_2)$, j(HONO), j(HCHO) etc. were obtained from solar UV spectra measured by actinic-flux spectroradiometry (Bohn et al., 2008). Both sets of $j(O^1D)$ and $j(NO_2)$ data were in agreement within 5%. A summary of the general conditions encountered during the PRD campaign is given in Table 3, which presents mean values for the morning at 06:00–10:00 CNST and afternoon at 12:00–16:00 CNST (CNST = Chinese Standard Time = UTC + 8 h) over the days when HO_X measurements are available.

2.2 Radical measurements

OH, HO_2 and k_{OH} were measured by a compact laser-induced fluorescence (LIF) system built at Forschungszentrum Jülich, Germany (Fig. 2). The technique was initially developed for measurement of OH (Holland et al., 1995, 1998; Hofzumahaus et al., 1996) and was later extended by an additional measurement capability for HO_2 (Holland et al., 2003). The LIF instrument used at PRD is a follow-up version of the earlier system. It is designed to be smaller and more light-weight than the previous instrument, making the instrument easier to handle in field applications (e.g., Kleffmann et al., 2005; Schlosser et al., 2009). Furthermore, the newly developed LP-LIF (laser-flash photolysis laser-induced fluorescence) technique for measurement of k_{OH} was implemented (Lou et al., 2010) utilizing the same tunable laser source for OH detection. In the following, the LIF system for HO_X detection will be described briefly, explaining the general principle and technical differences between this and the earlier instrument version.

Radicals are sampled by expansion of ambient air through an inlet nozzle (0.4 mm orifice, Beam-Dynamics) into a low pressure (3.5 mbar) chamber, where OH is detected by LIF at 308 nm. HO_2 is monitored in a separate parallel detection chamber, in which HO_2 is first chemically converted to OH by reaction with injected NO, followed by LIF detection of OH. It should be noted that the two detection cells are mechanically connected by a set of laser-baffle arms, but are separated by a quartz window preventing any possible contamination of the OH cell by NO from the HO_2 cell. The two detection chambers share one dry-vaccuum pump (IPX500, BOC-Edwards) and are constantly purged by a background flow of pure nitrogen through the detection cell (1 slpm; slpm = litre per minute at 1 atm, 298 K) and through the baffle arms (0.2 slpm). In each detection chamber, the gas expansion produces a gas beam through the center of the cell, which is irradiated at right angle by a 308 nm laser beam (8–10 mm diameter) from a pulsed narrow-bandwidth UV laser system operated at a repetition rate of 8.5 kHz. The laser wavelength can be tuned, in order to selectively excite OH electronically on a single OH absorption line, here the $Q_1(3)$ line of the $A^2\Sigma^+(v' = 0) - X^2\Pi\ (v'' = 0)$

vibronic band at 308 nm. OH resonance fluorescence emitted between 307 nm and 311 nm is collected by an assembly of large-diameter fused-silica lenses and narrow-band optical filters and is detected with a highly sensitive channel photomultiplier tube which is mounted perpendicular to the gas beam and the laser axis. The fluorescence is measured by gated photon counting using a time delay (≈ 50 ns) to discriminate the longer-lived OH fluorescence (150 ns lifetime at 3.5 hPa) from the instantaneous laser stray light (≈ 20 ns duration). The signals are further corrected for solar straylight, which enters the measurement cells through the nozzle orifice and is measured after each laser-pulse in a separate time gate with a delay of 25 µs. Furthermore, the laser is tuned periodically on- and off-resonance to distinguish the OH fluorescence signal from non-resonant laser excited background signals (Hofzumahaus et al., 1996). The amount of detected OH fluorescence integrated over successive laser pulses can be converted into an ambient radical concentration, of which the required sensitivity is determined by calibration (see below).

The major technical differences between the present and previous instrument version is the integration of more compact, light-weight components for the laser system, the vacuum pumps and the gated photon-counting system and a more convenient distribution of the 308 nm laser radiation by optical fibres rather than by beam-steering mirrors. The laser system used in this work consists of an intracavity frequency-doubled tunable dye-laser (Tintura, New Laser Generation) which is pumped by a frequency-doubled Nd-YAG laser (Navigator-I, Spectra Physics). The dye laser uses an intracavity etalon for line narrowing and provides a stable laser bandwidth (7 GHz at 308 nm). This stability is an advantage compared to the previously used laser system where the bandwidth was very sensitive to laser alignment with corresponding need for frequent recalibration of the HO_X measurement. The present laser system provides up to 100 mW of UV (308 nm) pumped by a laser power of about 4 W (532 nm). The 308 nm power is distributed between the HO_X detection cells, the LP-LIF instrument and the wavelength reference cell by means of beam splitters in a ratio of 60 : 32 : 8. Due to a technical problem of the frequency-doubling device of the Nd-YAG laser during the field campaign, the total UV power was reduced to 60 mW in the beginning, decreasing further to 10 mW towards the end of the campaign. The laser radiation was delivered by a 6 m long optical multimode fibre (QMMJ-55HP-UVVIS-200/240 µ, AMS Technologies) with an effective transmission of about 50–70% to the detection cells. In- and outcoupling of the laser beam was achieved by AR-coated plano-convex quartz lenses ($f = 25$ mm and 50 mm, respectively). For fluorescence detection, gated channel-photomultipliers (C1943P, Perkin Elmer) were connected to a gated photon-counter card (PMS300, Becker und Hickl GmbH) and gating signals were provided by a digital delay generator (DDG, Becker und Hickl GmbH) triggered by the laser system. The dry-vaccum pump (IPX500, BOC-Edwards) is connected to each detection chamber by separate flexible metal-bellow tubes (40 mm diameter) including motorized butterfly valves (MKS153), in order to stabilize the pressure in the cells to better than ± 0.1 mbar.

During the PRD campaign, the laser was tuned periodically to on- and off-resonance wavelength positions with integration times of 40 s and 8 s, respectively. Including some overhead time for laser scanning, a typical time resolution of 40–70 s was achieved for the HO_X measurements. The instrument was calibrated with known amounts of OH and HO_2 radicals which were generated in a flow of synthetic air by photolysis of water vapor at 185 nm from a low-pressure discharge mercury lamp (for details, see Holland et al., 2003; Fuchs et al., 2011). The calibration source was recently tested in intercomparisons against absolute measurement techniques for OH (Schlosser et al., 2006, 2009), confirming the estimated accuracy (±10%, 1σ) of the calibration method. At PRD, successive calibration measurements showed an unusally large 1σ variability by 8.7% and 13.6% for OH and HO_2, respectively, from day to day. This variability is about a factor of two larger than usual and suggests uncontrolled changes of the instrumental detection sensitivity. Since no trend was observed in the calibration data, an average calibration factor was applied for the campaign. The observed variability adds to the calibration uncertainty which is estimated to be 20% (1σ) in total. OH and HO_2 interferences caused by ambient O_3 were corrected by an amount of $(6 \pm 2) \times 10^3\ \mathrm{cm}^{-3}$ and $2 \times 10^4\ \mathrm{cm}^{-3}$, respectively, per ppb of ozone. The detection limit of the 5 min averaged OH data is 5×10^5 cm^{-3} before 18 July 2006, afterwards due to a reduced laser power, this number increased to 1×10^6 cm^{-3}; the detection limit of the 5 min averaged HO_2 data is $(1-2) \times 10^6$ cm^{-3} before 18 July 2006, $(2-3) \times 10^6$ cm^{-3} afterwards.

2.3 HO_2 measurement interference by RO_2

Recent laboratory studies show that our HO_2 detection system exhibits a significant sensitivity to specific RO_2 species, which are converted to OH by a sequence of NO dependent reactions (Nehr et al., 2011; Fuchs et al., 2011). In general, RO_2 reacts in the gas expansion with the injected NO as fast as HO_2 and forms RO (Reaction R5). In case of simple alkoxy radicals, RO reacts predominantly with O_2 and produces HO_2 (Reaction R6). Because of the short reaction time (few milliseconds) and the strongly reduced O_2 number density in the gas expansion, the RO to HO_2 conversion is slow and the following production of detectable OH is marginal. Experimental tests have shown that the corresponding interference by C_1–C_4 alkyl peroxy radicals is generally not larger than about 5% (Stevens et al., 1994; Kanaya et al., 2001; Tan et al., 2001; Creasey et al., 2002; Holland et al., 2003; Ren et al., 2004), consistent with the new results by Fuchs et al. (2011). However, in case of RO_2 from OH reactions with alkenes and aromatics, the RO radicals formed in Reaction (R5) undergo unimolecular reactions and extremely fast decomposition to HO_2. In this case, the NO-dependent Reactions (R5) and (R7) control the effective rate of $RO_2 \rightarrow HO_2 \rightarrow OH$ conversion. A significant amount of RO_2 is eventually detected as OH in the HO_2 detection cell, resulting in relative detection sensitivities (α_{RO_2}) for specific RO_2 compared to HO_2 of larger than 50% (Nehr et al., 2011; Fuchs et al., 2011).

Experimental α_{RO_2} values for peroxy radicals from selected VOCs of the groups of alkanes, alkenes, aromatics and OVOCs are shown in Fig. 3 (red symbols). They apply to the instrumental configuration used at PRD (Fuchs et al., 2011). Relative detection sensitivities for methyl peroxy and ethyl peroxy radicals are small with 4% and 7%, respectively; but values are larger for peroxy radicals from cyclohexane (48%), simple alkenes (85–95%), isoprene (79%), and benzene (86%). Also the peroxy radicals from the OH reactions with major isoprene degradation products, methyl vinyl ketone (MVK) and methacrolein (MACR), have significant α_{RO_2} values of about 60%.

Model simulations of α_{RO_2} are also presented in Fig. 3 (blue symbols). They are based on the Master Chemical Mechanism MCM v3.1 (Saunders et al., 2003; Jenkin et al., 2003) and reproduce the trend of the experimental values reasonably well (Fuchs et al., 2011). The simulations are shown for the major VOCs which contributed more than 95% to the VOC reactivity at PRD. The HO_2 concentration measured by LIF, denoted as $[HO_2^*]$, is then expected to be the sum of the true HO_2 concentration and a systematic bias from the mixture of RO_2 species i which are detected with different relative sensitivities $\alpha^i_{RO_2}$.

$$[HO_2^*]=[HO_2]+\Sigma\left(\alpha^i_{RO_2}\times[RO_2]_i\right) \tag{1}$$

We have not attempted to correct the measured HO_2^* values in order to obtain true HO_2 concentrations, since RO_2 concentration measurements and their speciation are not available. However, a chemical box model is used to calculate concentrations for both HO_2 and HO_2^* (see below). The difference between these two concentrations can be considered an estimate of the effective instrumental interference from RO_2 at the conditions found at PRD.

2.4 The model

A zero-dimensional chemical box model was used to calculate concentrations of OH, HO_2, HO_2^* and photochemical products of nitrogen and carbon compounds. In this work, we call the applied chemical mechanism RACM-MIM-GK. It is based on the Regional Atmospheric Chemical Mechanism (RACM) (Stockwell et al., 1997) which was upgraded with the isoprene degradation scheme by Karl et al. (2006). The latter scheme is a modified version (26 reactions) of the mechanism by Geiger et al. (2003), who prepared a condensed version of the Mainz Isoprene Mechanism (MIM, 44 reactions) (Pöschl et al., 2000). The complete mechanism of RACM-MIM-GK, which has been used before by Hofzumahaus et al. (2009) and Lou et al. (2010), is reported in Table S1 in the Supplement of this paper.

The model calculations were constrained to measurements of O_3, HONO, NO, NO_2, CO, CH_4, C_3–C_{12} VOCs, photolysis frequencies, water vapor, ambient temperature and pressure. Table 2 explains the distribution of the measured VOC species into the lumped RACM-MIM-GK categories. Concentrations of ethane and ethene were set to fixed values of 1.5 ppb and 3 ppb, respectively, estimated from a few canister samples. The H_2 mixing ratio was assumed to be 550 ppb. The model was operated in a time-dependent mode with 5-min time resolution and 2 days spin-up time. An additional loss process with a lifetime of 24 h was assumed for calculated species, in order to represent dry deposition in the model. The lifetime corresponds to an assumed deposition velocity of 1.2 $\mathrm{cm\,s^{-1}}$ and a well-mixed boundary layer height of about 1 km. Numerical sensitivity tests showed that the assumed deposition lifetime has a relatively small influence on the reactivity of the modelled oxidation products (e.g. OVOCs) (Lou et al., 2010). As a result, calculated OH and HO_2 concentrations vary by less than 5% and 10%, respectively, if the deposition rate is changed by a factor of two. Further sensitivity studies were performed to propagate the errors from the model boundary conditions and the reaction rate constants of RACM-MIM-GK (Hofzumahaus et al., 2009) resulting in error estimates of about 40% for the calculated OH, HO_2 and HO_2^* concentrations.

For the calculation of HO_2^*, we used the $\alpha^i_{RO_2}$ values which are listed for the major RACM peroxy radical species in Table 4. For RO_2 from OH reaction with CH_4 (methane), ETH (ethane), ETE (ethene), ISO (isoprene), MVK and MACR, the experimental data from Fig. 3 were used directly. For HC3, the experimental value of ETH was adopted, because the model predicted $\alpha^i_{RO_2}$ values are almost equal for the respective peroxy radicals (Fig. 3). For HC5 and HC8, $\alpha^i_{RO_2}$ was assumed to be the same as the experimental value for cyclohexane. For the peroxy radicals of OLI and

OLT, the measured value for propene was used and for the aromatics TOL and XYL, the measured $\alpha^{i}_{\mathrm{RO_2}}$ for benzene was applied.

In the following, model runs with the RACM-MIM-GK are used as a reference which represents the framework of established photochemistry with classical, NO-dependent radical recycling. This base-case is denoted as M0. To explore possible reaction mechanisms which recycle OH radicals without NO, additional model runs were performed which incorporate assumed generic reaction pathways (M1–M2) or newly proposed mechanisms (M3–M6) into RACM-MIM-GK. Furthermore, the results from RACM-MIM-GK are compared to model runs based on the detailed MCM v3.1 (M7). An overview of the different model scenarios is given in Table 5 and the corresponding reaction mechanisms are listed in the Supplement of this paper. Details and results of the sensitivity runs are given in Sect. 4.3.

3 Results

3.1 Observations of HO_X and other photochemical parameters

During PRIDE-PRD2006, concentrations of OH and HO_2^* were measured from 5 to 25 July 2006. An overview of the 5 min-averaged data is shown in Fig. 4. Data gaps were caused by heavy rain during the typhoon BILIS (15–17 July 2006), by electric power failure (22 July 2006), and by instrument calibration or maintenance (i.e. 11 and 18 July 2006). The diurnal variations of the observed radicals followed a regular pattern from day to day, with maximum values around noon. To evaluate the variability of the daily peak values, mean values of the upper 0.05 percentiles of OH and HO_2^* were calculated for each day. Daily maximum OH concentrations varied from $15\times10^{6}\,\mathrm{cm^{-3}}$ to $26\times10^{6}\,\mathrm{cm^{-3}}$, while daily maximum HO_2^* concentrations varied from 3×10^{8} to $25\times10^{8}\,\mathrm{cm^{-3}}$. Significant HO_X concentrations were measured during nighttime as well. While individual OH data points lie close to the limit of detection, hourly averaged nighttime values (at solar zenith angles larger than 90°) were in the range of

$0.2 \times 10^6\,\text{cm}^{-3}$ to $5 \times 10^6\,\text{cm}^{-3}$ with an error of $0.2 \times 10^6\,\text{cm}^{-3}$. When averaged over the whole campaign, the mean nighttime value was $2 \times 10^6\,\text{cm}^{-3}$. For HO_2^* the hourly averaged nighttime values were in the range of $0.1 \times 10^8\,\text{cm}^{-3}$ to $10 \times 10^8\,\text{cm}^{-3}$ with an uncertainty of $0.1 \times 10^8\,\text{cm}^{-3}$. Over the whole campaign, the mean nighttime value of HO_2^* was $2 \times 10^8\,\text{cm}^{-3}$. The origin of nighttime HO_X will be analyzed in a separate publication.

In order to characterize the encountered air masses from a photochemical point of view, time series of important parameters influencing the radical concentrations are presented in Fig. 5. $j(O^1D)$ and $j(NO_2)$ showed regular diurnal patterns with high noontime values that reached up to $4 \times 10^{-5}\,\text{s}^{-1}$ and $1 \times 10^{-2}\,\text{s}^{-1}$, respectively. Relatively small daytime values were observed on 15–17 July 2006 when the sky was covered by a dark cloud layer during typhoon BILIS. High concentrations of NO (often more than 10 ppb) were measured in the morning hours, while low concentrations below 1 ppb prevailed in the afternoon. Anthropogenic emissions from heavy-duty cars and combustion activities after midnight might be the cause for the morning peak of NO, whereas a ban of heavy duty cars during daytime, the enlarged boundary layer height and photochemical oxidation of NO_x may be the reason for the low NO concentrations in the afternoon. The diurnal characteristic of NO_2 is similar to that of NO, but large concentrations of NO_2 often appear near midnight probably produced by titration of O_3 with freshly emitted NO. Ozone showed an anti-correlated diurnal variation compared to NO_2. Peak values of O_3 mostly appear around noon or afternoon hours, indicating local photochemical ozone production (Lu et al., 2010). Relatively high concentrations of HONO were observed at the PRD site during early morning hours (about 1 ppb) and noon time (about 200 ppt). Details of the HONO budget will be discussed by Li et al. (2011). CO concentrations had typical noontime values around 400 ppb. Spikes in the CO data set indicate scattered sources and inhomogeneities of the advected air mass. This is consistent with observed biomass burning activities close to the site and in the PRD region as a whole.

Since the site is located in a forested region, large isoprene concentrations can appear during daytime. As discussed by Lou et al. (2010), daily peak isoprene concentrations were correlated to the wind direction. For the prevailing southerly wind direction, the air had to travel over a large water reservoir and daily peak isoprene concentration were typically 1–2 ppb. For northerly wind directions (13–14 July and 23–25 July 2006), emissions from nearby plants or agriculture fields could directly influence the site and daily peak isoprene concentrations approached 5–6 ppb then. A biomass burning event on 23–25 July 2006 was identified by analysis of measured optical aeorosol properties (Garland et al., 2008; Rose et al., 2010). Thus, the high isoprene concentration during this event could also have been caused by stress-induced plant emissions.

3.2 Base-case model results for HO_X

Model calculated results (M0) for OH and HO_2^* are compared to the measured time series in Fig. 4. For OH, the base-case model shows diurnal patterns that are systematically different from the observations. During morning hours, modelled and measured concentrations always agree well, while in the afternoon the model underestimates the observed OH by a factor of 2 to 8. On the other hand, observations of HO_2^* are much better reproduced by the model. This picture using the full time resolution of observed data is consistent with what has been reported previously (Hofzumahaus et al., 2009) using diurnally averaged boundary conditions for modelling (see also Fig. S1 in the Supplement).

The model has been used to simulate both ambient HO_2 and measured HO_2^*, which are shown in Fig. 4 for comparison. The difference between the two quantities can be considered a model estimate of the HO_2 interference from ambient RO_2. It is quite small during morning hours, while it becomes larger in the afternoon going along with notable day to day variability. On average, the model estimated interference is about 30% at daytime. It should be noted that this estimate is model dependent and has a large uncertainy since the model cannot reproduce the observed OH correctly (see Sect. 4.3).

Title Page
Abstract Introduction
Conclusions References
Tables Figures
◀◀ ▶▶
◀ ▶
Back Close
Full Screen / Esc
Printer-friendly Version
Interactive Discussion

The radical budget of HO_x and the related RO_x is analyzed in Figs. 6 and 7 using chemical turnover rates determined by the base model (M0). Figure 6 shows the mean diurnal profiles of the production and loss rates of RO_x. During daytime, the primary OH production, P(OH), and primary HO_2 production, $P(HO_2)$, were the dominant part of $P(RO_X)$. O_3 and HONO photolysis reactions constituted the major part of P(OH), while HCHO photolysis (about 3–4 ppb h^{-1} during noon time) dominated $P(HO_2)$. The next important processes were the photolysis of dicarbonyls including gloxyal (GLY), α-carbonyl aldehydes (MGLY) and unsaturated dicarbonyls (DCB). In the early morning, HONO photolysis was the most important primary source of HO_X, which contributed 60–70% of $P(HO_X)$ between 07:00 and 08:00 CNST. A recently proposed new primary OH source, the reaction of excited NO_2 with H_2O (Li et al., 2008), has been examined as well. The photolysis frequency for the production of excited NO_2 was calculated from measured actinic flux spectra, assuming that excited NO_2 is formed beyond the photodissociation threshold (420 nm) up to wavelength of 700 nm with unity quantum yield. The estimated radical production rate from this channel was only about 0.1 ppb h^{-1} at 08:30 CNST (SZA = 60°) which is almost negligible at our conditions. As indicated by the overlapping grey dashed and red solid lines in Fig. 6a, the total RO_X production is balanced by equally large RO_X sinks, $L(RO_X)$, in the model. As shown by Fig. 6b, $L(RO_X)$ is dominated in the morning by OH reactions with odd nitrogen compounds and RO_2 reactions with NO_x yielding nitrates and PANs. In the afternoon, self reactions of HO_2 or RO_2 and cross reactions between HO_2 and RO_2 are dominant. The radical chemistry is VOC limited in the morning and NO_X limited in the afternoon with the transition taking place around 10:00–11:00 CNST.

In Fig. 7a,b, the rates of OH reactions yielding HO_2 and RO_2 are specified. As discussed for the correspondingly measured k_{OH} (Lou et al., 2010), half of the OH loss can be explained by the measured trace gases given in Table 1 and half by modelled daughter products of isoprene, alkenes and aromatics. OH → HO_2 conversion is mainly caused by reaction of OH with CO and formaldehyde throughout the day. During early morning hours, the total OH → RO_2 conversion rate is dominated by oxidation reactions of alkenes (propene, butenes, pentenes) and aromatics (styrene, toluene, xylenes, trimethylbenzenes), while it is dominated by isoprene and its degradation products in the afternoon. This is reflected in the RO_2 speciation within different NO_X regimes (see Fig. S2 and Table S4, Supplement).

Recycling rates for $RO_2 \rightarrow HO_2$ and $HO_2 \rightarrow OH$ are speciated in Fig. 7c,d, respectively. $RO_2 \rightarrow HO_2$ conversion is dominated by NO reactions with MO2, ISOP and MACP. Here, MO2 is predominantly formed from oxidation of methane, isoprene and alkenes. Figure 7d shows that $HO_2 \rightarrow OH$ recycling (red line) is mainly caused by the reaction $HO_2 + NO$ (blue line). It is nearly balanced by HO_2 formation through $OH \rightarrow HO_2$ plus $RO_2 \rightarrow HO_2$ reactions (dark red line), demonstrating that the HO_2 budget is mainly controlled by cycling reactions rather than by primary production and termination reactions. Furthermore, it can be noted that the total peroxy radical formation rate, i.e. the sum of $R(OH \rightarrow HO_2)$ and $R(OH \rightarrow RO_2)$ (violet dashed line) agrees most of the day with the recyling rate $HO_2 \rightarrow OH$. A relative large difference is found only in the afternoon, indicating inefficient recycling to OH in the RO_X propagation implemented in the base model, consistent with the analysis of $L(RO_X)$ in Fig. 6b.

4 Discussion

HO_X concentrations observed during PRIDE-PRD2006 are the highest so far reported for urban and suburban environments at summer time (Table 6). In Mexico City (located at a similar latitude and also in a developing country) relative small HO_X concentrations were observed. Among the other cities, which are located in developed countries like US, Europe and Japan, measurements at Nashville and New York City showed relative high HO_X concentrations that approach the levels of PRD. One reason for the high radical concentrations at PRD is the strong subtropical insolation leading to large radical production rates by photolysis (cf. Fig. 6a). In fact, the mean noontime $j(O^1D)$ value was larger during PRIDE-PRD2006 than during other campaigns listed in Table 6. The meteorological conditions and high precursor concentrations (e.g., O_3, water vapor, HONO) favored large HO_X radical concentrations. Taking into account the high mean OH reactivity of $20\,s^{-1}$ observed at Guangzhou during daytime, the large measured OH concentrations indicate exceptional intense photochemistry in Southern China. The significant model underprediction of OH in the afternoon (Fig. 4) implies that the known OH sources alone cannot explain the high OH daytime values. In order to characterize the missing chemical processes that sustain the high experimental OH values, the discrepancies between modelled and measured OH will be investigated in the following discussion as a function of other atmospheric parameters.

When comparing the reported HO_2 values in Table 6, it must be kept in mind that the data from different campaigns were measured by similar LIF techniques, which all rely on chemical HO_2 conversion. It is likely that the interference from specific RO_2 species, described in Sect. 2.3, has influenced all LIF measurements of HO_2 compiled in Table 6. Since the abundance and speciation of RO_2 is certainly different for the various campaigns, a relatively large, not well quantified uncertainty has to be attached to the HO_2 comparison among different locations.

4.1 $j(O^1D)$ and NO_X dependence of OH

A high correlation between OH and $j(O^1D)$ was observed over the whole range of atmospheric conditions during the PRD campaign, with a linear correlation coefficient of $r^2 = 0.81$ (Fig. 8a). In past campaigns, similar high correlations were observed (Rohrer and Berresheim, 2006, and reference therein), but at conditions with much lower VOC reactivities. For limiting cases with low or high NO_x concentrations, theoretical explanations were attempted using reaction schemes with a simplified VOC chemistry (e.g., Poppe et al., 1995). But even for the limiting cases in the steady state calculation of OH, the role of other photolysis processes (e.g. of HCHO and NO_2) is clearly visible and should in principle disturb the linear correlation between OH and $j(O^1D)$. Ehhalt and Rohrer (2000) performed a detailed analysis of this relationship based on observational results derived during the POPCORN campaign in rural Germany. They showed that the observed correlation of OH and $j(O^1D)$ is just fortuitously linear, resulting from the combined influence of all photolytic processes on OH, which are highly correlated among themselves. According to this analysis, a power-law function with an exponential parameter close to unity is more suitable. Based on the analysis of a five year OH dataset, a simple empirical model was constructed to describe this relation (Rohrer and Berresheim, 2006):

$$[\mathrm{OH}] = a \times (j(\mathrm{O}^1\mathrm{D})/10^{-5}\,\mathrm{s}^{-1})^b + c \tag{2}$$

The pre-exponential coefficient, a, incorporates the condensed information of the chemical conditions (e.g. NO_x or VOCs) at a certain location. Exponent b reflects the combined effects of all photolytic processes (i.e. $j(O^1D)$, $j(NO_2)$, j(HONO), j(HCHO)). These photolytic processes either play a role in primary production processes of HOx radicals or influence its recycling processes. Finally, the offset parameter c accounts for non-photolytic OH sources. When applied to the scatter plot in Fig. 8a, a Levenberg-Marquard fit yields $a = 5.6 \times 10^6\,\mathrm{cm}^{-3}$, $b = 0.68$ and $c = 2.3 \times 10^6\,\mathrm{cm}^{-3}$, providing a parameterized description for the PRD conditions.

For comparison to other campaigns, a linear fit is more appropriate, since often only linear coefficients are published. The disadvantage in using linear coefficients is a shortfall in the description of twilight conditions for OH. The slope of a linear fit to the PRIDE-PRD2006 observations is $4.0 \times 10^{11}\,\mathrm{s\,cm}^{-3}$ and the offset $2.4 \times 10^6\,\mathrm{cm}^{-3}$. In the marine boundary layer, reported slopes are relatively low, $\leq 2 \times 10^{11}\,\mathrm{s\,cm}^{-3}$ (Berresheim et al., 2003; Brauers et al., 2001; Smith et al., 2006), while in continental regions reported values lie in the range of $(2–4) \times 10^{11}\,\mathrm{s\,cm}^{-3}$ (Holland et al., 2003; Rohrer and Berresheim, 2006; Ehhalt and Rohrer, 2000). The slope for PRIDE-PRD2006 is at the upper limit of previous continental field observations, which again indicates an intense photochemical activity in the PRD region.

The model simulation (M0) cannot reproduce the high correlation between measured OH and $j(O^1D)$. Unlike the experimental scatter plot (Fig. 8a), the plot of calculated OH versus measured $j(O^1D)$ is split into two groups of data forming a "V"-like shape

(Fig. 8b). The upper branch corresponds to morning hours, when modelled and observed OH are in good agreement (cf., Fig. 4). The lower branch of the "V" represents afternoon data, when the model severely underpredicts OH. One major difference between the two branches is the level of NO_x, which was high in the morning and low in the afternoon (Table 3). Interestingly, the empirical relationship between measured OH and $j(O^1D)$ is not only compact in both NO_x regimes, but both subsets of data also overlap completely (Fig. 8a). Apparently, some unknown chemical mechanism which is missing in the base model stabilizes the ambient OH concentration. A similar tendency was noticed for a measured five-year OH record at Hohenpeissenberg, where the observed correlation between OH and $j(O^1D)$ was more stable and compact than could be explained by a chemical box model (Rohrer and Berresheim, 2006).

For inspection of the OH dependence on NO_X, we remove the strong influence of $j(O^1D)$ by normalization as shown in Eq. (3).

$$[\mathrm{OH_{Jnorm}}] = \frac{[\mathrm{OH}]}{j(\mathrm{O^1D})} \times \overline{j(\mathrm{O^1D})} \tag{3}$$

Here, $\overline{j(O^1D)}$ denotes the mean value of the $j(O^1D)$ data set. To avoid using conditions during twilight for reasons discussed above, the data in this normalization analysis are restricted to $j(O^1D)$ larger than $1 \times 10^{-5}\,s^{-1}$. The NO_X dependency of observed and model calculated OH_{Jnorm} are denoted as small dots in Fig. 8c,d, respectively. In addition, trend lines are shown that were obtained by averaging OH_{Jnorm} concentrations over equal $\ln([NO_X]/ppb)$ intervals of 0.5.

The mean measured OH_{Jnorm} is almost constant over the displayed NO_X range, showing a broad curvature with a relative maximum of about $15 \times 10^6\,cm^{-3}$ at 3–4 ppb NO_X (Fig. 8c). The observed NO_X dependency differs considerably from the model simulation which predicts a steady increase of OH from low values at less than 1 ppb NO_X to a maximum OH concentration at about 10 ppb NO_X (Fig. 8d). Agreement of the observed and modelled OH_{Jnorm} data is found only at the high end of observed NO_X levels. This behaviour is completely different from the results in relatively clean rural air at POPCORN, where a nonlinear dependence with a maximum at 1 ppb NO_2 was found in good agreement for measured and modelled OH (Ehhalt, 1999).

4.2 NO and isoprene dependence of the measured-to-modelled OH ratio

To gain further insight into the shortcomings of the base model calculation M0, the ratio of measured-to-modelled OH, OH_{obs}/OH_{mod}, has been inspected as a function of NO, CO and VOCs. A notable trend is found only for NO and isoprene (Fig. 9a,b), with correlation coefficients $r = -0.77$ and $r = 0.48$, respectively. Figure 9a displays a strong NO dependence of OH_{obs}/OH_{mod} with a smooth transition from ratios of about 8 at 0.02 ppb NO to unity ratio at NO mixing ratios larger than 1 ppb. This indicates that chemical processes are missing in the model which compete with NO dependent reactions and become dominant at low NO.

With respect to isoprene, two data clouds around 1 ppb and 3 ppb of isoprene are visible in Fig. 9b. For the combined data set, a weak positive correlation between OH_{obs}/OH_{mod} and isoprene seems to exist. No correlation is found for other investigated parameters. For example, indicators of anthropogenic activities like CO (especially from biomass burning) or benzene clearly show no correlation with OH_{obs}/OH_{mod} (Fig. 9c,d).

Figure 10a offers a more detailed inspection of the relationship between OH_{obs}/OH_{mod} and isoprene by color coding the data according to the concurrently measured NO mixing ratios. It can be seen that part of the trend of OH_{obs}/OH_{mod} vs. isoprene can be attributed to an anticorrelation between NO and isoprene. Isoprene was generally lower in the morning when NO was high and reached highest values in the afternoon when the NO mixing ratio was small. When the data in Fig. 10a are selected for low NO (< 0.5 ppb), no significant trend with isoprene is found (red circles). Thus, the weak positive correlation in the whole data set between OH_{obs}/OH_{mod} and isoprene seems to be a consequence of the different NO_X levels of the two data clouds around 1 ppb and 3 ppb of isoprene. Given the small dynamic range of isoprene and the influence of NO, a functional dependence on isoprene cannot be postulated on the basis of our PRD data.

A model underprediction of measured OH concentrations by up to an order of magnitude has been reported for forested areas, which are characterized by isoprene emissions and low NO_x (Tan et al., 2001; Ren et al., 2008; Lelieveld et al., 2008; Pugh et al., 2010; Whalley et al., 2011). Figure 10b compares our OH_{obs}/OH_{mod} ratios with the results from these other studies. For this purpose, we use the PRD data selected for low NO (< 0.5 ppb) from Fig. 10a (red circles). The magnitude of the measured-to-modelled OH ratios of our study agree well with those from previous investigations, i.e. above deciduous forest in North-America during PROPHET (Tan et al., 2001) and INTEX-A (Ren et al., 2008), above the Amazonian rainforest during GABRIEL (Kubistin et al., 2010) and the Borneo rainforest during OP3 (Whalley et al., 2011). When all data sets are combined, a consistent trend of an OH model underprediction with increasing isoprene seems to emerge, as pointed out previously by Ren et al. (2008) and Kubistin et al. (2010).

While the experimental OH data from the different campaigns were measured by similar LIF techniques, differences exist in the chemical models that were applied for the OH simulations. Four different chemical mechanisms were used: RACM-MIM-GK for our study, RACM supplemented with a detailed isoprene chemistry and explicit ozonolysis of terpene (Tan et al., 2001) for PROPHET, MIM (Pöschl et al., 2000) for GABRIEL, and a lumped mechanism described by Crawford et al. (1999) for INTEX-A. For OP3, OH was calculated by an analytical equation with experimentally determined parameters under photostationary steady-state assumptions. The trend in Fig. 10b is apparently independent of the specific model used for OH prediction. It suggests that an OH source mechanism is missing in current models which is related to biogenic emissions or to their photochemical daughter products. Anthropogenic VOCs made also a significant contribution to the OH reactivity at PRD (Lou et al., 2010), but their variability is too small to allow a positive identification of an influence on the OH model underprediction at PRD.

4.3 Model modifications to explain the observed HO_x

4.3.1 Additional radical recycling

In a previous study, Hofzumahaus et al. (2009) compared the experimental OH loss rate ($k_{OH} \times [OH]$), calculated from measured concentrations and reactivities of OH, with the major known OH sources from photolysis of O_3 and HONO (P_{OH}) and radical recycling ($k_{HO_2+NO}[NO][HO_2]$) for PRIDE-PRD2006. The OH loss and production rates were found to be balanced in the morning when HO_2 was efficiently recycled to OH, but a significant OH source was missing in the afternoon at low NO. Several generic reaction pathways were tested that may explain the mismatch within the OH budget. In that paper, observed OH and HO_2 concentrations were utilized as target parameters for comparison with the model results. The most simple candidate for a new reaction pathway, which quantitatively explains the observations, was $RO_2 + X \longrightarrow HO_2$ in combination with $HO_2 + X \longrightarrow OH$ (Table 5, M1). This is the same type of reactions as those of peroxy-radicals with NO. Assuming rate constants as for the NO reactions, a concentration of 0.8 ppb was needed for X to match the mean diurnal profiles of both HO_X species.

Since then, a strong interference in the HO_2 measurements by LIF from RO_2 was discovered (Fuchs et al., 2011, see Sect. 2.3). For this reason, the published results of the PRD campaign concerning the HO_X budget have to be reevaluated. The previous major conclusion was that the recycling term $k_{HO_2+NO}[NO][HO_2]$ in the OH budget was too small to explain the observed total OH loss rate. Since the interference of HO_2 by RO_2 has one direction, namely the enlargement of HO_2^* with respect to the true HO_2, the conclusion that additional OH recycling is missing in the model is still valid. Furthermore, the arguments made for the selection of the generic reaction terms with X still hold. However, a formerly excluded generic reaction type, a single reaction $HO_2 + Y \longrightarrow OH$ (Table 5, M2), has to be reconsidered. Before, M2 was ruled out, because the modelled HO_2 became much smaller than the measurement (HO_2^*) when the simulated OH was matched to the observed OH. Since ambient HO_2 is smaller than HO_2^* and we have no experimental constraint on RO_2, results from model M2 can now be matched to the observations of both OH and HO_2^*.

Figure 11 shows the mean diurnal variations of the modelled OH, HO_2, HO_2^* and RO_2 calculated by the RACM-GK-MIM model without (M0) and with additional radical recycling (M1, M2). The results for OH and HO_2^* are also compared to the measured data. In case of M0, there is agreement between modelled and measured OH in the morning, but a large discrepancy exists in the afternoon as discussed previously (Hofzumahaus et al., 2009). The modelled HO_2^* is about 30% larger than the modelled HO_2 and is in very good agreement with the measurement (HO_2^*). Yet, even the modelled HO_2 is not significantly different from the measurement, given the combined experimental and model uncertainties (Hofzumahaus et al., 2009).

In model runs M1 and M2, the concentrations of the unknown reactants X and Y were optimized for half-hourly bins to achieve a best fit to the observed OH in the time interval 10:00–18:00 CNST (Fig. 11). Agreement is also achieved for modelled and measured HO_2^* within the combined uncertainties. Thus, both types of additional recycling scenarios (M1, M2) provide acceptable generic solutions to describe the observed HO_x data.

Regarding the M1 case, the modelled HO_2^* is about 30% larger than the modelled HO_2 like in the base case (M0). In both cases, the RO_2/HO_2 ratio is close to one and about half of the RO_2 species contribute significantly to the interference in the measured HO_2. In the M2 calculation there is a huge difference of more than an order of magnitude between modelled HO_2 and HO_2^*. The reason are very large calculated RO_2/HO_2 ratios with values of 10–60 and corresponding ISOP/HO_2 ratios of 2–15 during the afternoon hours. The large difference of the RO_2/HO_2 ratios between mechanism M1 and M2 would be a tool to distinguish which recycling type provides a more realistic description. However, experimental data of RO_2/HO_2 ratios are not available for PRD and are also generally scarce in literature. In previous campaigns, Matrix Isolation Electron Spin Resonance (MIESR) has been applied to measure directly peroxy radicals in forested and suburban environments. RO_2/HO_2 ratios were observed to vary from <1 to 5 (Mihelcic et al., 2003). The ratio RO_2/HO_2 has also been investigated by measurement techniques that apply chemical conversion, including LIF, peroxy radical chemical amplifiers (PERCA) and chemical ionization mass spectrometry (CIMS). Here, ratios of 4–15 were reported for a remote mountain site in Colorado (Stevens et al., 1997), <1–9 for a rural area near Berlin (Platt et al., 2002), about 0.5 for a rural area in Pennsylvania (Ren et al., 2003), 1–3 for the free troposphere above Burkina Faso (Andrés-Hernández et al., 2010), about one for a remote mountain site in Italy (Hanke et al., 2002) and <1–2 for the polluted outflow from Mexico City and Asian countries (Hornbrook et al., 2011). As reported by Fuchs et al. (2011) and Hornbrook et al. (2011), HO_2 measurement techniques like LIF or CIMS are susceptible to interferences from specific RO_2 radicals that are produced by atmospheric oxidation of alkenes, dialkenes like isoprene, and aromatics. Thus, the reported RO_2/HO_2 ratios determined by these techniques were probably underestimated. Furthermore, to our knowledge, the RO_2/HO_2 ratio has never been determined experimentally for conditions like in this study with k_{OH} well above $15\,s^{-1}$. In conclusion, previously reported values of ambient RO_2/HO_2-ratios do not allow to choose between scenarios M1 and M2.

4.3.2 Mechanistic chemistry updates

As outlined in the introduction, a number of new chemical mechanisms have been proposed recently to explain the large model underprediction of OH observed in forested areas. Here, we test how well these OH regenerating mechanisms explain the discrepancy between modelled and measured OH at PRD. An overview of the tested mechanisms M3–M6 is given in Table 5. In addition, we show model results of the detailed MCMv3.1 (M7), which contains a more explicit description of the VOC chemistry compared to RACM-GK-MIM (M0). The corresponding model results for OH, HO_2, HO_2^* and RO_2 and the measured OH and HO_2^* data are compared for M0 and M3–M7 in Fig. 12.

The implementation of additional OH formation from the reaction of HO_2 with acyl peroxy and β-keto peroxy radicals (Hasson et al., 2004; Jenkin et al., 2007; Dillon and Crowley, 2008) (M3) and with epoxide peroxy radicals (Paulot et al., 2009) (M4) has only a marginal impact on the modelled concentrations of OH, HO_2, HO_2^* and RO_2. For each species, the modelled curves (Fig. 12) of the different scenarios M0, M3 and M4 are virtually indistinguishable. The reason for the small sensitivity to the $RO_2 + HO_2$ reactions is the dominating influence of the competing peroxy radical reactions with NO given average mixing ratios of more than 0.2 ppb NO at PRD.

The mechanisms M5 and M6 calculate significantly larger OH concentrations than M0. The model M5 includes the isoprene chemistry LIM0 postulated by Peeters and Müller (2010), whereas M6 contains additional OH formation by reaction of ISOP with HO_2 as proposed by Lelieveld et al. (2008) and Butler et al. (2008). Both mechanisms contain an “amplification” factor generating additional radicals within the radical recycling processes. In the LIM0 mechanism, amplification is achieved by the photolysis of HPALDs, which are assumed to have a yield of about one OH and one HO_2 (M5a), or alternatively up to three OH plus one HO_2 (M5b). The M6 scenario has two variants with yields of two (M6a) and four (M6b) OH radicals. Among the different M5 and M6 scenarios, M5b gives the largest increase of modelled OH by about a factor of two in the afternoon, relative to the M0 calculation. However, there is still a significant gap compared to the experimental data. The model explains only 40–50% of the measured OH values during the afternoon at PRD, while it reproduces 70–90% of the observed OH for the GABRIEL and INTEX-A campaigns (Stavrakou et al., 2010). In scenario M6b modelled OH increases on average by a factor of 1.7 in the afternoon, reaching only 30–40% of the observed OH concentration. The same mechanism, however, was able to explain the GABRIEL and OP3-1 results by increasing the modelled OH by up to an order of magnitude (Lelieveld et al., 2008; Kubistin et al., 2010; Pugh et al., 2010). The different OH enhancements for PRIDE-PRD2006 and GABRIEL using M5b or M6b are caused by the different levels of NO, which were an order of magnitude larger at PRD compared to the Amazonian rain forest. At PRD, the competing peroxy radical reactions with NO decrease the sensitivity to radical amplification that is postulated in the mechanisms M5b and M6b.

The M5 and M6 scenarios calculate HO_2^* values that are larger than in the base case and overpredict the observed data by a factor 1.2–1.4. The modelled RO_2 is close to the corresponding HO_2 concentrations at daytime, so that the RO_2 to HO_2 ratio seems to be relatively independent of the chemical mechanisms used (M0, M3–M6). Table S7 in the Supplement shows that the relative contributions of speciated RO_2 radicals is not responding very much to changing OH concentrations. Thus, the difference between modelled HO_2 and HO_2^* is 20–40% for M3–M6, close to the 30% difference in M0.

An additional model calculation was performed using the well established MCMv3.1 (Saunders et al., 2003; Jenkin et al., 2003) (M7). The calculated results for OH, HO_2, HO_2^* and RO_2 agree well with the reference model (M0) especially at afternoon (Fig. 12). This demonstrates that the OH underprediction by RACM-GK-MIM is not specifically caused by the lumped representation of the VOC chemistry, but is a fundamental deficit in our current understanding of tropospheric chemistry.

4.3.3 NO dependence of model predictions

Two possible concepts have been discussed above to explain the difference between modelled (M0) and observed OH at PRIDE-PRD2006. One concept introduces generic reactions with unknown species driving additional radical recycling (M1, M2). The other concept relies on the implementation of peroxy-peroxy radical reactions that produce additional OH rather than acting as a radical sink (M3–M6). The potential of each mechanism to explain the observed OH at PRD is compared in Fig. 13 as a function of NO at daytime conditions ($j(O^1D) > 1 \times 10^{-5}\,s^{-1}$). It is apparent that all mechanisms reproduce the measured OH reasonably well at NO concentrations above 1 ppb, while the spread among the model predictions is largest at the low end of the NO scale. Not surprisingly, the generic mechanisms M1 and M2 show good agreement over the whole NO dynamical range, as a consequence of the numerical fitting of the unknown reactants X and Y (cf. Fig. 11). The NO dependent trend of the M3–M6 predictions is caused by peroxy radical reactions with NO, which compete with peroxy-peroxy radical reactions and become dominant at NO levels above 1 ppb.

Among the mechanisms M3–M6, the LIM0 mechanism (M5b) and the proposed OH recycling by reaction ISOP + HO_2 (M6b) offer the largest potential to brigde the gap between modelled (M0) and measured OH at low NO. Considering an estimated accuracy for OH_{obs}/OH_{mod} of 45%, calculated by error propagation of the corresponding experimental and model uncertainties, the remaining discrepancy of a factor of two at NO < 0.2 ppb is still significant. The postulated mechanisms M5 and M6 are not yet confirmed by laboratory experiments. Thus, the remaining discrepancies in Fig. 13 may be due to the uncertainty of these mechanisms, or indicate other, so far unidentified processes that increased OH at PRD.

Figure 13 also shows the modelled OH reactivity (M0) given by CO and VOCs, and its breakdown into different subgroups of organic components for each of the NO bins. The modelled reactivity has an almost constant value of 20 s^{-1} over the NO range of two orders of magnitude. Over the whole range of NO, isoprene was never dominant making a contribution of 10–16% to the organic reactivity. However, together with its first generation of daughter products (OISO), isoprene made a significant reactivity contribution that increased towards lower NO values.

4.3.4 Heterogeneous radical loss

HO_2 radicals may be lost by heterogeneous uptake onto aerosol particles when competing gas-phase reactions of HO_2 are relatively slow. The potential influence of heterogeneous loss has been examined in model sensitivity studies mainly for marine environments (e.g., Carslaw et al., 1999, 2002; Sommariva et al., 2006; Kanaya et al., 2000, 2007a). Up to a factor of two of HO_2 reduction was simulated when the heterogeneous uptake coefficient for marine aerosol was assumed to be maximum, $\gamma = 1$ (Sommariva et al., 2006; Kanaya et al., 2007a). During PRIDE-PRD2006, the daytime (08:00–18:00) averaged aerosol surface-area density was very large, about 1400 $\mu m^2\,cm^{-3}$ (Li et al., 2011). Assuming free molecular transport and $\gamma = 0.5$, the heterogeneous reactivity is calculated to be 0.1 s^{-1} in comparison to 0.025 s^{-1} by NO. Implementing this heterogeneous loss rate into model M0 causes a reduction of the calculated HO_2 by 50%. This implies that a heterogeneous uptake process has the potential to reduce HO_2 at PRD significantly. However, the estimated strong influence is speculative. Though laboratory studies with Cu-II doped aqueous particles have shown large accomodation coefficients close to one (see overview, Kolb et al., 2010), measurements at salt solutions, soot and wet organic particles showed much smaller effective uptake coefficients in the range 0.01–0.1 (e.g., Thornton and Abbatt, 2005; Bedjanian et al., 2005; Taketani et al., 2009, 2010). Furthermore, the influence of heterogeneous uptake will be strongly diminished by competing HO_2 reactions which are required as additional OH sources (e.g., $HO_2 + X$). If HO_2 is heterogeneously lost, it will decrease the OH concentration as well. Alternatively, one could speculate about a heterogeneous reaction of HO_2 on particles that releases OH (or an OH precursor) into the gas-phase. However, the potential HO_2 reactivity towards aerosol is at least a factor of five too small compared the required reactivity to match the observed OH (cf. Fig. 11g, scenario M2). Thus, it seems unlikely that a surface-catalyzed HO_2 to OH recycling process is the missing OH source.

4.4 OH radical budget analysis

Experimental and modelled (M0–M7) parameters that characterize the HO_x chemistry during the afternoon hours 12:00–16:00 CNST at PRD are compared in Table 7. The main body of the table shows reaction rates that are relevant for the budget of OH and HO_2, and the bottom gives radical parameters such as the mean concentration and reactivity of OH, as well as the RO_2/HO_2 and HO_2/OH ratios. It can be noted that the models M0 (RACM-GK-MIM), M3, M4 and M7 (MCMv3.1) yield almost identical values for each parameter, mostly within 10%.

Following the OH budget analysis by Hofzumahaus et al. (2009), the total OH loss rate, $D(OH)$, given by $[OH] \times k_{OH}$ is compared to the total OH production rate, $P'(OH)$

(top of the table). Here, P'(OH) is calculated from the photolysis of ozone and HONO, and from OH recycling by $HO_2 + NO$. Using solely experimental data, a missing OH source of about 25 ppb/hr is calculated. However, the recently detected interference in the HO_2 measurement introduces a systematic error. If the measured HO_2 data are corrected by −30% as estimated by model M0, then the missing OH source is calculated to be 10% larger, having a value of about 27 ppb h^{-1}. If the measured HO_2^* would be dominated by RO_2 (as predicted by model M2), then the missing OH source would have a 20% larger value of at most 30 ppb h^{-1}.

The models M0 and M7 show a small difference of about 2 ppb h^{-1} between D(OH) and P'(OH) (Table 7), which is caused by minor OH sources. These include ozonolysis of alkenes, photolysis of peroxides, OH recycling by $HO_2 + O_3$ and prompt OH regeneration, e.g. from ISHP + OH. In case of the model scenarios M2–M6, the difference between D(OH) and P'(OH) is larger than in the base case (M0), owing to the additional OH sources implemented in each different mechanism. The respective source strengths are largest for M1 and M2, because they were fitted to match the observed OH. In the other models, the additional source strengths are not sufficient to match the observed OH. Models M3 and M4 have only marginal effects on the total OH production, whereas the scenarios M5b and M6b provide the most efficient additional OH sources among the newly proposed chemical mechanisms. It is interesting to note that the postulated OH formation from HPALD photolysis (M5b) is a factor of 1.6 more efficient than the corresponding photolysis of ozone and HONO. Since the HPALD photolysis is also expected to produce HO_2 (Peeters and Müller, 2010), the contribution from HPALD photolysis to the HO_X radical pool would actually be larger than from the sum of photolysis rates of O_3, HONO, and HCHO.

The proposed additional OH sources in M1–M6 all rely an radical recycling without oxidation of NO to NO_2. Thus, they do not contribute to photochemical ozone formation. This is reflected by the $P(O_3)/[OH] \times k_{OH}$ ration (Table 7), where $P(O_3)$ denotes the ozone production rate from the reactions of HO_2 and RO_2 with NO. While the established mechanism M0 and M7 predict a ratio of one for the conditions at PRD, a strongly reduced ozone production efficiency is expected from M1 and M2. In case of the scenarios M5b and M6b, a reduction of 30% is calculated. The large variability of the calculated ozone production efficiency between the different mechanisms demonstrates that the insufficient understanding of the radical recycling mechanism also introduces a significant uncertainty in the predictions of secondary pollutants.

5 Conclusions

Ambient OH and HO_2 concentrations were measured by LIF during the PRIDE-PRD2006 campaign at a rural site downwind of Guangzhou in the Pearl River Delta in summer 2006. The most obvious feature of the HO_X photochemistry for this campaign was published by Hofzumahaus et al. (2009). A large imbalance between the experimentally determined total OH loss rate and production of OH from known radical sources was discovered, indicating a missing OH source at conditions of high isoprene (2 ppb) and low NO (0.1–0.2 ppb). A generic reaction pathway, $RO_2 + X \rightarrow HO_2$ and $HO_2 + X \rightarrow OH$ was proposed to enable a chemical model to reproduce both the observed OH and HO_2 concentrations. In this work, we have reevaluated the dataset and extended the model analysis, taking into account a newly discovered artefact in the LIF measurement of HO_2. The major findings are:

1. Considering the interference from RO_2 in the HO_2 detection channel, the need for an additional $HO_2 \rightarrow OH$ recycling process persists. Since the true HO_2 concentration is smaller than the measured value HO_2^*, the missing OH source may be up to 85% of the OH loss rate rather than 74% calculated previously. Moreover, the need of an adjacent recycling $RO_2 \rightarrow HO_2$ to match the observed HO_2 has diminished, since the measured HO_2 data contain a contribution from RO_2 that is not known quantitatively. The concentrations of individual RO_2 species would be needed for a correction of the interference which is not attainable in retrospect.

2. Daily maxima of OH and HO_2^* were in the range of (15–26) × 10^6 cm^{-3} and (3–25) × 10^8 cm^{-3}, respectively. Compared to previously reported measurements in other urban and suburban areas, the OH concentrations at PRD are among the highest values so far reported. Measured HO_2 concentrations reported in the literature are difficult to compare, because they were obtained by LIF techniques and likely influenced by unspecified interferences from RO_2 similar to our case.

3. The observed OH showed a consistent high correlation with $j(O^1D)$ over a broad range of NO_x conditions. The correlation cannot be reproduced by model simulations, indicating that OH stabilizing processes are missing in current models (e.g., RACM-MIM-GK).

4. The observed OH exhibited only a weak dependence on NO_x in contrast to model predictions. While modelled and measured OH agree well at NO mixing ratios above 1 ppb, a continuously increasing underprediction of the observed OH is found towards lower NO concentrations, reaching a factor of 8 at 0.02 ppb NO.

5. A dependence of the modelled-to-measured OH ratio on isoprene cannot be derived from the PRD data set due to the relatively small isoprene variability. However, the magnitude of the ratio fits into the isoprene dependent trend that was reported from other campaigns in forested regions.

6. Two recently postulated isoprene mechanisms (Lelieveld et al., 2008; Peeters and Müller, 2010) lead to significant enhancements of OH expected for PRD, but an underprediction of the observed OH by a factor of 2 remains at low NO. If the photolysis of HPALDs is as efficient as proposed in the LIM0 mechanism by Peeters and Müller (2010), the corresponding OH formation at PRD would be more important than the primary OH production from ozone and HONO.

The isoprene mechanisms by Lelieveld et al. (2008) and Peeters and Müller (2010) have shown potential to explain the unexpectedly large OH concentrations observed above forests during the GABRIEL and INTEX-A campaigns. The still significant underprediction of OH at the NO concentration regime of PRD may be explained either by the uncertainties of the postulated mechanisms which are not yet confirmed by laboratory studies, or by other so far unidentified OH sources that may have played a role. Further experimental investigations will be needed to get a full picture of the radical chemistry in VOC rich environments. Improved measurement techniques for HO_2 and (speciated) RO_2 would be extremely helpful in future studies to gain more insight into the cycling of radicals and its impact on tropospheric photochemistry.

Supplementary material related to this article is available online at: http://www.atmos-chem-phys-discuss.net/11/11311/2011/ acpd-11-11311-2011-supplement.pdf.

Acknowledgements. We thank the PRIDE-PRD2006 campaign team (2002CB410801), especially F. Yang, H. Su, A. Nowak, N. Takegawa, and A. Oebel for help and support at the field site. We thank P. H. Xie, Anhui Institute of Optics and Fine Mechanics in Hefei, China, for providing the methane data.

References

Andrés-Hernández, M. D., Stone, D., Brookes, D. M., Commane, R., Reeves, C. E., Huntrieser, H., Heard, D. E., Monks, P. S., Burrows, J. P., Schlager, H., Kartal, D., Evans, M. J., Floquet, C. F. A., Ingham, T., Methven, J., and Parker, A. E.: Peroxy radical partitioning during the AMMA radical intercomparison exercise, Atmos. Chem. Phys., 10, 10621–10638, doi:10.5194/acp-10-10621-2010, 2010. 11339

Archibald, A. T., Cooke, M. C., Utembe, S. R., Shallcross, D. E., Derwent, R. G., and Jenkin, M. E.: Impacts of mechanistic changes on HO_x formation and recycling in the oxidation of isoprene, Atmos. Chem. Phys., 10, 8097–8118, doi:10.5194/acp-10-8097-2010, 2010. 11318, 11319

Atkinson, R.: Atmospheric reactions of alkoxy and β-hydroxyalkoxy radicals, Int. J. Chem. Kinet., 29, 99–111, 1997. 11315

Bedjanian, Y., Lelievre, S., and Le Bras, G.: Experimental study of the interaction of HO_2 radicals with soot surface, Phys. Chem. Chem. Phys., 7, 334–341, 2005. 11343

Berresheim, H., Plass-Dülmer, C., Elste, T., Mihalopoulos, N., and Rohrer, F.: OH in the coastal boundary layer of Crete during MINOS: Measurements and relationship with ozone photolysis, Atmos. Chem. Phys., 3, 639–649, doi:10.5194/acp-3-639-2003, 2003. 11333

Bohn, B., Corlett, G. K., Gillmann, M., Sanghavi, S., Stange, G., Tensing, E., Vrekoussis, M., Bloss, W. J., Clapp, L. J., Kortner, M., Dorn, H.-P., Monks, P. S., Platt, U., Plass-Dülmer, C., Mihalopoulos, N., Heard, D. E., Clemitshaw, K. C., Meixner, F. X., Prevot, A. S. H., and Schmitt, R.: Photolysis frequency measurement techniques: results of a comparison within the ACCENT project, Atmos. Chem. Phys., 8, 5373–5391, doi:10.5194/acp-8-5373-2008, 2008. 11320

Brasseur, G. P., Prinn, R. G., and Pszenny, A. P. (Eds.): Atmospheric Chemistry in a Changing World, The IGBP Series, Springer, Berlin, 2003. 11314

Brauers, T., Hausmann, M., Bister, A., Kraus, A., and Dorn, H. P.: OH radicals in the boundary layer of the Atlantic Ocean 1. Measurements by long-path laser absorption spectroscopy, J. Geophys. Res., 106, 7399–7414, 2001. 11333

Butler, T. M., Taraborrelli, D., Brühl, C., Fischer, H., Harder, H., Martinez, M., Williams, J., Lawrence, M. G., and Lelieveld, J.: Improved simulation of isoprene oxidation chemistry with the ECHAM5/MESSy chemistry-climate model: lessons from the GABRIEL airborne field campaign, Atmos. Chem. Phys., 8, 4529–4546, doi:10.5194/acp-8-4529-2008, 2008. 11318, 11340, 11363

Carslaw, N., Creasey, D. J., Heard, D. E., Lewis, A. C., McQuaid, J. B., Pilling, M. J., Monks, P. S., Bandy, B. J., and Penkett, S. A.: Modeling OH, HO_2, and RO_2 radicals in the marine boundary layer – 1. Model construction and comparison with field measurements, J. Geophys. Res., 104, 30241–30255, 1999. 11342

Carslaw, N., Creasey, D., Heard, D., Jacobs, P., Lee, J., Lewis, A., Bauguitte, S., Penkett, S., Monks, P., and Salisbury, G.: Eastern Atlantic Spring Experiment 1997 (EASE97) 2. Comparisons of model concentrations of OH, HO_2, and RO_2 with measurements, J. Geophys. Res., 107, 4190, doi:10.1029/2001JD001568, 2002. 11342

Chan, C. K. and Yao, X.: Air pollution in mega cities in China, Atmos. Environ., 42, 1–42, 2008. 11317, 11320

Crawford, J., Davis, D., Olson, J., Chen, G., Liu, S., Gregory, G., Barrick, J., Sachse, G., Sandholm, S., Heikes, B., Singh, H., and Blake, D.: Assessment of upper tropospheric HO_x

sources over the tropical Pacific based on NASA GTE/PEM data: net effect on HO_x and other photochemical parameters, J. Geophys. Res., 104, 16255–16273, 1999. 11336

Creasey, D. J., Heard, D. E., and Lee, J. D.: Eastern Atlantic Spring Experiment 1997 (EASE97) 1. Measurements of OH and HO_2 concentrations at Mace Head, Ireland, J. Geophys. Res., 107(D10), 4091, doi:10.1029/2001JD000892, 2002. 11324

Crosley, D. R.: The measurement of OH and HO_2 in the atmosphere, J. Atmos. Sci., 52, 3299–3314, 1995. 11316

Dillon, T. J. and Crowley, J. N.: Direct detection of OH formation in the reactions of HO_2 with $CH_3C(O)O_2$ and other substituted peroxy radicals, Atmos. Chem. Phys., 8, 4877–4889, doi:10.5194/acp-8-4877-2008, 2008. 11318, 11340

Dusanter, S., Vimal, D., Stevens, P. S., Volkamer, R., Molina, L. T., Baker, A., Meinardi, S., Blake, D., Sheehy, P., Merten, A., Zhang, R., Zheng, J., Fortner, E. C., Junkermann, W., Dubey, M., Rahn, T., Eichinger, B., Lewandowski, P., Prueger, J., and Holder, H.: Measurements of OH and HO_2 concentrations during the MCMA-2006 field campaign – Part 2: Model comparison and radical budget, Atmos. Chem. Phys., 9, 6655–6675, doi:10.5194/acp-9-6655-2009, 2009. 11315

Ehhalt, D. H.: Photooxidation of trace gases in the troposphere, Phys. Chem. Chem. Phys., 1, 5401–5408, 1999. 11315, 11335

Ehhalt, D. H. and Rohrer, F.: Dependence of the OH concentration on solar UV, J. Geophys. Res., 105, 3565–3571, 2000. 11332, 11333

Emmerson, K. M., Carslaw, N., Carpenter, L. J., Heard, D. E., Lee, J. D., and Pilling, M. J.: Urban atmospheric chemistry during the PUMA campaign 1: Comparison of modelled OH and HO_2 concentrations with measurements, J. Atmos. Chem., 52, 143–164, 2005. 11364

Emmerson, K. M., Carslaw, N., Carslaw, D. C., Lee, J. D., McFiggans, G., Bloss, W. J., Gravestock, T., Heard, D. E., Hopkins, J., Ingham, T., Pilling, M. J., Smith, S. C., Jacob, M., and Monks, P. S.: Free radical modelling studies during the UK TORCH Campaign in Summer 2003, Atmos. Chem. Phys., 7, 167–181, doi:10.5194/acp-7-167-2007, 2007. 11315, 11364

Finlayson-Pitts, B. J. and Pitts, Jr., J. N.: Chemistry of the Upper and Lower Atmosphere: Theory, Experiments and Applications, Academic Press, San Diego, 2000. 11314

Fuchs, H., Bohn, B., Hofzumahaus, A., Holland, F., Lu, K. D., Nehr, S., Rohrer, F., and Wahner, A.: Detection of HO_2 by laser-induced fluorescence: calibration and interferences from RO_2 radicals, Atmos. Meas. Tech. Discuss., 4, 1255–1302, doi:10.5194/amtd-4-1255-2011, 2011. 11319, 11323, 11324, 11325, 11337, 11339, 11368

Garland, R. M., Yang, H., Schmid, O., Rose, D., Nowak, A., Achtert, P., Wiedensohler, A., Takegawa, N., Kita, K., Miyazaki, Y., Kondo, Y., Hu, M., Shao, M., Zeng, L. M., Zhang, Y. H., Andreae, M. O., and Pöschl, U.: Aerosol optical properties in a rural environment near the mega-city Guangzhou, China: implications for regional air pollution, radiative forcing and remote sensing, Atmos. Chem. Phys., 8, 5161–5186, doi:10.5194/acp-8-5161-2008, 2008. 11329

Geiger, H., Barnes, I., Bejan, I., Benter, T., and Spittler, M.: The tropospheric degradation of isoprene: an updated module for the regional atmospheric chemistry mechanism, Atmos. Environ., 37, 1503–1519, 2003. 11325

George, L. A., Hard, T. M., and O'Brien, R. J.: Measurement of free radicals OH and HO_2 in Los Angeles smog, J. Geophys. Res., 104, 11643–11655, 1999. 11364

Hallquist, M., Wenger, J. C., Baltensperger, U., Rudich, Y., Simpson, D., Claeys, M., Dommen, J., Donahue, N. M., George, C., Goldstein, A. H., Hamilton, J. F., Herrmann, H., Hoffmann, T., Iinuma, Y., Jang, M., Jenkin, M. E., Jimenez, J. L., Kiendler-Scharr, A., Maenhaut, W., McFiggans, G., Mentel, Th. F., Monod, A., Prévôt, A. S. H., Seinfeld, J. H., Surratt, J. D., Szmigielski, R., and Wildt, J.: The formation, properties and impact of secondary organic aerosol: current and emerging issues, Atmos. Chem. Phys., 9, 5155–5236, doi:10.5194/acp-9-5155-2009, 2009. 11315

Hanke, M., Uecker, J., Reiner, T., and Arnold, F.: Atmospheric peroxy radicals: ROXMAS, a new mass-spectrometric methodology for speciated measurements of HO_2 and ΣRO_2 and first results, Int. J. Mass Spectrom., 213, 91–99, 2002. 11339

Harrison, R. M., Yin, J., Tilling, R. M., Cai, X., Seakins, P. W., Hopkins, J. R., Lansley, D. L., Lewis, A. C., Hunter, M. C., Heard, D. E., Carpenter, L. J., Creasey, D. J., Lee, J. D., Pilling, M. J., Carslaw, N., Emmerson, K. M., Redington, A., Derwent, R. G., Ryall, D., Mills, G., and Penkett, S. A.: Measurement and modelling of air pollution and atmospheric chemistry in the U.K. West Midlands conurbation: overview of the PUMA Consortium project, Sci. Total Environ., 360, 5–25, 2006. 11364

Hasson, A. S., Tyndall, G. S., and Orlando, J. J.: A product yield study of the reaction of HO_2 radicals with ethyl peroxy ($C_2H_5O_2$), acetyl peroxy ($CH_3C(O)O_2$), and acetonyl peroxy ($CH_3C(O)CH_2O_2$) radicals, J. Phys. Chem. A, 108, 5979–5989, 2004. 11318, 11340

Heard, D. E. and Pilling, M. J.: Measurement of OH and HO_2 in the troposphere, Chem. Rev., 103, 5163–5198, 2003. 11316

Hofzumahaus, A., Aschmutat, U., Heßling, M., Holland, F., and Ehhalt, D. H.: The measurement of tropospheric OH radicals by laser-induced fluorescence spectroscopy during the POPCORN field campaign, Geophys. Res. Lett., 23, 2541–2544, 1996. 11321

Hofzumahaus, A., Rohrer, F., Lu, K., Bohn, B., Brauers, T., Chang, C. C., Fuchs, H., Holland, F., Kita, K., Kondo, Y., Li, X., Lou, S., Shao, M., Zeng, L., Wahner, A., and Zhang, Y.: Amplified trace gas removal in the troposphere, Science, 324, 1702–1704, 2009. 11313, 11316, 11317, 11318, 11319, 11326, 11329, 11337, 11338, 11343, 11345, 11363

Holland, F., Heßling, M., and Hofzumahaus, A.: In situ measurement of tropospheric OH radicals by laser-induced fluorescence – a description of the KFA instrument, J. Atmos. Sci., 52, 3393–3401, 1995. 11321

Holland, F., Aschmutat, U., Heßling, M., Hofzumahaus, A., and Ehhalt, D. H.: Highly time resolved measurements of OH during POPCORN using laser-induced fluorescence spectroscopy, J. Atmos. Chem., 31, 205–225, 1998. 11321

Holland, F., Hofzumahaus, A., Schäfer, J., Kraus, A., and Pätz, H.-W.: Measurements of OH and HO_2 radical concentrations and photolysis frequencies during BERLIOZ, J. Geophys. Res., 108, 8246, doi:10.1029/2001JD001393, 2003. 11321, 11323, 11324, 11333, 11364

Hornbrook, R. S., Crawford, J. H., Edwards, G. D., Goyea, O., Mauldin III, R. L., Olson, J. S., and Cantrell, C. A.: Measurements of tropospheric HO_2 and RO_2 by oxygen dilution modulation and chemical ionization mass spectrometry, Atmos. Meas. Tech. Discuss., 4, 385–442, doi:10.5194/amtd-4-385-2011, 2011. 11339

Jenkin, M. E., Saunders, S. M., Wagner, V., and Pilling, M. J.: Protocol for the development of the Master Chemical Mechanism, MCM v3 (Part B): tropospheric degradation of aromatic volatile organic compounds, Atmos. Chem. Phys., 3, 181–193, doi:10.5194/acp-3-181-2003, 2003. 11325, 11341, 11363

Jenkin, M. E., Hurley, M. D., and Wallington, T. J.: Investigation of the radical product channel of the $CH_3C(O)O_2 + HO_2$ reaction in the gas phase, Phys. Chem. Chem. Phys., 9, 3149–3162, 2007. 11318, 11340

Jenkin, M. E., Hurley, M. D., and Wallington, T. J.: Investigation of the radical product channel of the $CH_3OCH_2O_2 + HO_2$ reaction in the gas phase, J. Phys. Chem. A, 114, 408–416, 2010. 11318

Kanakidou, M., Seinfeld, J. H., Pandis, S. N., Barnes, I., Dentener, F. J., Facchini, M. C., Van Dingenen, R., Ervens, B., Nenes, A., Nielsen, C. J., Swietlicki, E., Putaud, J. P., Balkanski, Y., Fuzzi, S., Horth, J., Moortgat, G. K., Winterhalter, R., Myhre, C. E. L., Tsigaridis, K., Vignati, E., Stephanou, E. G., and Wilson, J.: Organic aerosol and global climate modelling:

a review, Atmos. Chem. Phys., 5, 1053–1123, doi:10.5194/acp-5-1053-2005, 2005. 11315

Kanaya, Y., Sadanaga, Y., Matsumoto, J., Sharma, U. K., Hirokawa, J., Kajii, Y., and Akimoto, H.: Daytime HO_2 concentrations at Oki Island, Japan, in summer 1998: comparison between measurement and theory, J. Geophys. Res., 105, 24205–24222, 2000. 11342

Kanaya, Y., Sadanaga, Y., Hirokawa, J., Kajii, Y., and Akimoto, H.: Development of a ground-based LIF instrument for measuring HO_x radicals: instrumentation and calibrations, J. Atmos. Chem., 38, 73–110, 2001. 11324

Kanaya, Y., Cao, R., Kato, S., Miyakawa, Y., Kajii, Y., Tanimoto, H., Yokouchi, Y., Mochida, M., Kawamura, K., and Akimoto, H.: Chemistry of OH and HO_2 radicals observed at Rishiri Island, Japan, in September 2003: missing daytime sink of HO_2 and positive nighttime correlations with monoterpenes, J. Geophys. Res., 112, D11308, doi:10.1029/2006JD007987, 2007a. 11342

Kanaya, Y., Cao, R. Q., Akimoto, H., Fukuda, M., Komazaki, Y., Yokouchi, Y., Koike, M., Tanimoto, H., Takegawa, N., and Kondo, Y.: Urban photochemistry in Central Tokyo: 1. Observed and modeled OH and HO_2 radical concentrations during the winter and summer of 2004, J. Geophys. Res., 112, D21312, doi:10.1029/2007JD008670, 2007b. 11315, 11316, 11364

Karl, M., Dorn, H.-P., Holland, F., Koppmann, R., Poppe, D., Rupp, L., Schaub, A., and Wahner, A.: Product study of the reaction of OH radicals with isoprene in the atmosphere simulation chamber SAPHIR, J. Atmos. Chem., 55, 167–187, 2006. 11325, 11363

Kleffmann, J., Gavriloaiei, T., Hofzumahaus, A., Holland, F., Koppmann, R., Rupp, L., Schlosser, E., Siese, M., and Wahner, A.: Daytime formation of nitrous acid: a major source of OH radicals in a forest, Geophys. Res. Lett., 32, L05818, doi:10.1029/2005GL022524, 2005. 11321

Kolb, C. E., Cox, R. A., Abbatt, J. P. D., Ammann, M., Davis, E. J., Donaldson, D. J., Garrett, B. C., George, C., Griffiths, P. T., Hanson, D. R., Kulmala, M., McFiggans, G., Pöschl, U., Riipinen, I., Rossi, M. J., Rudich, Y., Wagner, P. E., Winkler, P. M., Worsnop, D. R., and O' Dowd, C. D.: An overview of current issues in the uptake of atmospheric trace gases by aerosols and clouds, Atmos. Chem. Phys., 10, 10561–10605, doi:10.5194/acp-10-10561-2010, 2010. 11343

Kubistin, D., Harder, H., Martinez, M., Rudolf, M., Sander, R., Bozem, H., Eerdekens, G., Fischer, H., Gurk, C., Klüpfel, T., Königstedt, R., Parchatka, U., Schiller, C. L., Stickler, A., Taraborrelli, D., Williams, J., and Lelieveld, J.: Hydroxyl radicals in the tropical troposphere over the Suriname rainforest: comparison of measurements with the box model MECCA, Atmos. Chem. Phys., 10, 9705–9728, doi:10.5194/acp-10-9705-2010, 2010. 11318, 11336, 11340

Lelieveld, J., Butler, T. M., Crowley, J. N., Dillon, T. J., Fischer, H., Ganzeveld, L., Harder, H., Lawrence, M. G., Martinez, M., Taraborelli, D., and Williams, J.: Atmospheric oxidation capacity sustained by a tropical forest, Nature, 452, 737–740, 2008. 11313, 11316, 11336, 11340, 11346, 11363, 11365

Lewis, A. C., Hopkins, J. R., Carpenter, L. J., Stanton, J., Read, K. A., and Pilling, M. J.: Sources and sinks of acetone, methanol, and acetaldehyde in North Atlantic marine air, Atmos. Chem. Phys., 5, 1963–1974, doi:10.5194/acp-5-1963-2005, 2005. 11315

Li, S. P., Matthews, J., and Sinha, A.: Atmospheric hydroxyl radical production from electronically excited NO_2 and H_2O, Science, 319, 1657–1660, 2008. 11330

Li, X., Brauers, T., Shao, M., Garland, R. M., Wagner, T., Deutschmann, T., and Wahner, A.: MAX-DOAS measurements in southern China: retrieval of aerosol extinctions and validation using ground-based in-situ data, Atmos. Chem. Phys., 10, 2079–2089, doi:10.5194/acp-10-2079-2010, 2010. 11320

Li, X., Haeseler, R., Holland, F., Bohn, B., Hofumahaus, A., Rohrer, F., Wahner, A., Lu, K., Shao, M., Garland, R., Su, H., Nowak, A., Takegawa, N., Zhang, Y., and Brauers, T.: Exploring the atmospheric chemistry of nitrous acid (HONO) at a rural site in Southern China, in preparation, 2011. 11328, 11342

Lou, S., Holland, F., Rohrer, F., Lu, K., Bohn, B., Brauers, T., Chang, C. C., Fuchs, H., Häseler, R., Kita, K., Kondo, Y., Li, X., Shao, M., Zeng, L., Wahner, A., Zhang, Y., Wang, W., and Hofzumahaus, A.: Atmospheric OH reactivities in the Pearl River Delta – China in summer 2006: measurement and model results, Atmos. Chem. Phys., 10, 11243–11260, doi:10.5194/acp-10-11243-2010, 2010. 11315, 11317, 11320, 11321, 11326, 11329, 11330, 11336

Lu, K. D., Zhang, Y. H., Su, H., Shao, M., Zeng, L. M., Zhong, L. J., Xiang, Y. R., Chang, C. C., Chou, C. K. C., and Wahner, A.: Regional ozone pollution and key controlling factors of photochemical ozone production in Pearl River Delta during summer time, Sci. China Ser. B, 53, 651–663, 2010. 11328

Mao, J., Ren, X., Chen, S., Brune, W. H., Chen, Z., Martinez, M., Harder, H., Lefer, B., Rappenglück, B., Flynn, J., and Leuchner, M.: Atmospheric oxidation capacity in the summer of Houston 2006: comparison with summer measurements in other metropolitan studies, Atmos. Environ., 44, 4107–4115, doi:10.1016/j.atmosenv.2009.01.013, 2010. 11315, 11364

Martinez, M., Harder, H., Kovacs, T. A., Simpas, J. B., Bassis, J., Lesher, R., Brune, W. H., Frost, G. J., Williams, E. J., Stroud, C. A., Jobson, B. T., Roberts, J. M., Hall, S. R., Shetter, R. E., Wert, B., Fried, A., Alicke, B., Stutz, J., Young, V. L., White, A. B., and Zamora, R. J.: OH and HO_2 concentrations, sources, and loss rates during the Southern Oxidants Study in Nashville, Tennessee, summer 1999, J. Geophys. Res., 108, 4617, doi:10.1029/2003JD003551, 2003. 11364

Mihelcic, D., Holland, F., Hofzumahaus, A., Hoppe, L., Konrad, S., Müsgen, P., Pätz, H.-W., Schäfer, H.-J., Schmitz, T., Volz-Thomas, A., Bächmann, K., Schlomski, S., Platt, U., Geyer, A., Alicke, B., Perner, D., Klüpfel, T., and Moortgat, G. K.: Comparison of measurements and model calculations of OH, HO_2, and ΣRO_2 and the local ozone production during the BERLIOZ campaign, J. Geophys. Res., 108, 8254, doi:10.1029/2001JD001014, 2003. 11316, 11339

Monks, P. S., Granier, C., Fuzzie, S., Stohl, A., Williams, M., Akimoto, H., Ammani, M., Baklanov, A., Baltensperger, U., Bey, I., Blake, N., Blake, R., Carslaw, K., Cooper, O., Dentener, F., Fowler, D., Fragkou, E., Frost, G., Generoso, S., Ginoux, P., Grewe, V., Guenther, A., Hansson, H. C., Henne, S., Hjorth, J., Hofzumahaus, A., Huntrieser, H., Isaksen, I. S. A., Jenkin, M. E., Kaiser, J., Kanakidou, M., Klimont, Z., Kulmala, M., Laj, P., Lawrence, M., Lee, J., Liousse, C., Maione, M., McFiggans, G., Metzger, A., Mieville, A., Moussiopoulos, N., Orlando, J., O'Dowd, C., Palmer, P., Parrish, D., Petzold, A., Platt, U., Poeschl, U., Prévôt, A. S. H., Reeves, C. E., Reimann, S., Rudich, Y., Sellegri, K., Steinbrecher, R., Simpson, D., ten Brink, H., Theloke, J., van der Werf, G. R., Vautard, R., Vestreng, V., Vlachokostas, C., and von Glasow, R.: Atmospheric composition change – global and regional air quality, Atmos. Environ., 43, 5268–5350, 2009. 11314, 11316

Nehr, S., Bohn, B., Fuchs, H., and Hofzumahaus, A.: HO_2 formation from the OH + benzene reaction in the presence of O_2, Phys. Chem. Chem. Phys., in review, 2011. 11319, 11324

Paulot, F., Crounse, J. D., Kjaergaard, H. G., Kroll, J. H., Seinfeld, J. H., and Wennberg, P. O.: Isoprene photooxidation: new insights into the production of acids and organic nitrates, Atmos. Chem. Phys., 9, 1479–1501, doi:10.5194/acp-9-1479-2009, 2009. 11318, 11340, 11363, 11365

Peeters, J. and Müller, J.-F.: HO_x radical regeneration in isoprene oxidation via peroxy radical isomerisations. II: Experimental evidence and global impact, Phys. Chem. Chem. Phys., 12, 14227–14235, doi:10.1039/c0cp00811g, 2010. 11313, 11318, 11340, 11344, 11346, 11363, 11365

Peeters, J., Nguyen, T. L., and Vereecken, L.: HO_x radical regeneration in the oxidation of isoprene, Phys. Chem. Chem. Phys., 11, 5935–5939, 2009. 11318

Platt, U., Alicke, B., Dubois, R., Geyer, A., Hofzumahaus, A., Holland, F., Martinez, M., Mihelcic, D., Klupfel, T., Lohrmann, B., Patz, W., Perner, D., Rohrer, F., Schafer, J., and Stutz, J.: Free radicals and fast photochemistry during BERLIOZ, J. Atmos. Chem., 42, 359–394, 2002. 11339

Poppe, D., Zimmermann, J., and Dorn, H. P.: Field data and model-calculations for the hydroxyl radical, J. Atmos. Sci., 52, 3402–3407, 1995. 11332

Pöschl, U., von Kuhlmann, R., Poisson, N., and Crutzen, P. J.: Development and intercomparison of condensed isoprene oxidation mechanisms for global atmospheric modeling, J. Atmos. Chem., 37, 29–52, 2000. 11326, 11336

Pugh, T. A. M., MacKenzie, A. R., Hewitt, C. N., Langford, B., Edwards, P. M., Furneaux, K. L., Heard, D. E., Hopkins, J. R., Jones, C. E., Karunaharan, A., Lee, J., Mills, G., Misztal, P., Moller, S., Monks, P. S., and Whalley, L. K.: Simulating atmospheric composition over a South-East Asian tropical rainforest: performance of a chemistry box model, Atmos. Chem. Phys., 10, 279–298, doi:10.5194/acp-10-279-2010, 2010. 11316, 11318, 11336, 11340

Ren, X., Harder, H., Martinez, M., Lesher, R. L., Oliger, A., Shirley, T., Adams, J., Simpas, J. B., and Brune, W. H.: HO_x concentrations and OH reactivity observations in New York City during PMTACS-NY2001, Atmos. Environ., 37, 3627–3637, 2003. 11364

Ren, X., Harder, H., Martinez, M., Faloona, I. C., Tan, D., Lesher, R. L., Di Carlo, P., Simpas, J. B., and Brune, W. H.: Interference testing for atmospheric HO_x measurements by laser-induced fluorescence, J. Atmos. Chem., 47, 169–190, 2004. 11324

Ren, X., Olson, J. R., Crawford, J. H., Brune, W. H., Mao, J., Long, R. B., Chen, G., Avery, M. A., Sachse, G. W., Barrick, J. D., Diskin, G. S., Huey, L. G., Fried, A., Cohen, R. C., Heikes, B., Wennberg, P., Singh, H. B., Richard, D. R. B., and Shetter, E.: HO_x chemistry during INTEX-A 2004: observation, model calculations and comparison with previous studies, J. Geophys. Res., 113, D05310, doi:10.1029/2007JD009166, 2008. 11316, 11336

Ren, X., Edwards, G. D., Cantrell, C. A., Lesher, R. L., Metcalf, A. R., Shirley, T., and Brune, W. H.: Intercomparison of peroxy radical measurements at a rural site using laser-induced fluorescence and Peroxy Radical Chemical Ionization Mass Spectrometer (PerCIMS) techniques, J. Geophys. Res., 108, 4605, doi:10.1029/2003JD003644, 2003. 11339

Rohrer, F. and Berresheim, H.: Strong correlation between levels of tropospheric hydroxyl radicals and solar ultraviolet radiation, Nature, 442, 184–187, 2006. 11332, 11333, 11334

Rose, D., Nowak, A., Achtert, P., Wiedensohler, A., Hu, M., Shao, M., Zhang, Y., Andreae, M. O., and Pöschl, U.: Cloud condensation nuclei in polluted air and biomass burning smoke near the mega-city Guangzhou, China – Part 1: Size-resolved measurements and implications for the modeling of aerosol particle hygroscopicity and CCN activity, Atmos. Chem. Phys., 10, 3365–3383, doi:10.5194/acp-10-3365-2010, 2010. 11329

Saunders, S. M., Jenkin, M. E., Derwent, R. G., and Pilling, M. J.: Protocol for the development of the Master Chemical Mechanism, MCM v3 (Part A): tropospheric degradation of non-aromatic volatile organic compounds, Atmos. Chem. Phys., 3, 161–180, doi:10.5194/acp-3-161-2003, 2003. 11325, 11341, 11363

Schlosser, E., Bohn, B., Brauers, T., Dorn, H., Fuchs, H., Häseler, R., Hofzumahaus, A., Holland, F., Rohrer, F., Rupp, L. O., Siese, M., Tillmann, R., and Wahner, A.: Intercomparison of two hydroxyl radical measurement techniques at the atmosphere simulation chamber SAPHIR, J. Atmos. Chem., 56(2), 187–205, doi:10.1007/s10874-006-9049-3, 2006. 11323

Schlosser, E., Brauers, T., Dorn, H.-P., Fuchs, H., Häseler, R., Hofzumahaus, A., Holland, F., Wahner, A., Kanaya, Y., Kajii, Y., Miyamoto, K., Nishida, S., Watanabe, K., Yoshino, A., Kubistin, D., Martinez, M., Rudolf, M., Harder, H., Berresheim, H., Elste, T., Plass-Dülmer, C., Stange, G., and Schurath, U.: Technical Note: Formal blind intercomparison of OH measurements: results from the international campaign HOxComp, Atmos. Chem. Phys., 9, 7923–7948, doi:10.5194/acp-9-7923-2009, 2009. 11321, 11323

Shao, M., Lu, S., Liu, Y., Xie, X., Chang, C., Huang, S., and Chen, Z.: Volatile organic compounds measured in summer in Beijing and their role in ground-level ozone formation, J. Geophys. Res., 114, D00G06, doi:10.1029/2008JD010863, 2009. 11315

Shirley, T. R., Brune, W. H., Ren, X., Mao, J., Lesher, R., Cardenas, B., Volkamer, R., Molina, L. T., Molina, M. J., Lamb, B., Velasco, E., Jobson, T., and Alexander, M.: Atmospheric oxidation in the Mexico City Metropolitan Area (MCMA) during April 2003, Atmos. Chem. Phys., 6, 2753–2765, doi:10.5194/acp-6-2753-2006, 2006. 11316, 11364

Smith, S. C., Lee, J. D., Bloss, W. J., Johnson, G. P., Ingham, T., and Heard, D. E.: Concentrations of OH and HO_2 radicals during NAMBLEX: measurements and steady state analysis, Atmos. Chem. Phys., 6, 1435–1453, doi:10.5194/acp-6-1435-2006, 2006. 11333

Sommariva, R., Bloss, W. J., Brough, N., Carslaw, N., Flynn, M., Haggerstone, A.-L., Heard, D. E., Hopkins, J. R., Lee, J. D., Lewis, A. C., McFiggans, G., Monks, P. S., Penkett, S. A., Pilling, M. J., Plane, J. M. C., Read, K. A., Saiz-Lopez, A., Rickard, A. R., and

Williams, P. I.: OH and HO_2 chemistry during NAMBLEX: roles of oxygenates, halogen oxides and heterogeneous uptake, Atmos. Chem. Phys., 6, 1135–1153, doi:10.5194/acp-6-1135-2006, 2006. 11342

Stavrakou, T., Peeters, J., and Müller, J.-F.: Improved global modelling of HO_x recycling in isoprene oxidation: evaluation against the GABRIEL and INTEX-A aircraft campaign measurements, Atmos. Chem. Phys., 10, 9863–9878, doi:10.5194/acp-10-9863-2010, 2010. 11318, 11319, 11340

Steiner, A. L., Cohen, R. C., Harley, R. A., Tonse, S., Millet, D. B., Schade, G. W., and Goldstein, A. H.: VOC reactivity in central California: comparing an air quality model to ground-based measurements, Atmos. Chem. Phys., 8, 351–368, doi:10.5194/acp-8-351-2008, 2008. 11315

Stevens, P. S., Mather, J. H., and Brune, W. H.: Measurement of tropospheric OH and HO_2 by laser-induced fluorescence at low pressure, J. Geophys. Res., 99, 3543–3557, 1994. 11324

Stevens, P. S., Mather, J. H., Brune, W. H., Eisele, F., Tanner, D., Jefferson, A., Cantrell, C., Shetter, R., Sewall, S., Fried, A., Henry, B., Williams, E., Baumann, K., Goldan, P., and Kuster, W.: HO_2/OH and RO_2/HO_2 ratios during the Tropospheric OH Photochemistry Experiment: measurement and theory, J. Geophys. Res., 102, 6379–6391, 1997. 11339

Stockwell, W. R., Kirchner, F., Kuhn, M., and Seefeld, S.: A new mechanism for regional atmospheric chemistry modeling, J. Geophys. Res., 102, 25847–25879, 1997. 11325

Taketani, F., Kanaya, Y., and Akimoto, H.: Heterogeneous loss of HO_2 by KCl, synthetic sea salt, and natural seawater aerosol particles, Atmos. Environ., 43, 1660–1665, 2009. 11343

Taketani, F., Kanaya, Y., and Akimoto, H.: Kinetics of HO_2 Uptake in levoglucosan and polystyrene latex particles, J. Phys. Chem. Lett., 1, 1701–1704, 2010. 11343

Tan, D., Faloona, I., Simpas, J. B., Brune, W., and Shepson, P. B.: HO_x budgets in a deciduous forest: results from the PROPHET summer 1998 campaign, J. Geophys. Res., 106, 24,407, 2001. 11316, 11324, 11336

Taraborrelli, D., Lawrence, M. G., Butler, T. M., Sander, R., and Lelieveld, J.: Mainz Isoprene Mechanism 2 (MIM2): an isoprene oxidation mechanism for regional and global atmospheric modelling, Atmos. Chem. Phys., 9, 2751–2777, doi:10.5194/acp-9-2751-2009, 2009. 11365

Thornton, J. and Abbatt, J. P. D.: Measurements of HO_2 uptake to aqueous aerosol: mass accommodation coefficients and net reactive los, J. Geophys. Res., 110, D08309, doi:10.1029/2004JD005402, 2005. 11343

Thornton, J. A., Woolridge, P. J., Cohen, R. C., Martinez, M., Harder, H., Brune, W. H., Williams, E. J., Roberts, J. M., Fehsenfeld, F. C., Hall, S. R., Shetter, R. E., Wert, B. P., and Fried, A.: Ozone production rates as a function of NO_x abundances and HO_x production rates in the Nashville urban plume, J. Geophys. Res., 107, 4146, doi:10.1029/2001JD000932, 2002. 11316, 11364

Volkamer, R., San Martini, F., Molina, L. T., Salcedo, D., Jimenez, J. L., and Molina, M. J.: A missing sink for gas-phase glyoxal in Mexico City: formation of secondary organic aerosols, Geophys. Res. Lett., 34, L19807, doi:10.1029/2007GL030752, 2007. 11315

Whalley, L. K., Edwards, P. M., Furneaux, K. L., Goddard, A., Ingham, T., Evans, M. J., Stone, D., Hopkins, J. R., Jones, C. E., Karunaharan, A., Lee, J. D., Lewis, A. C., Monks, P. S., Moller, S. J., and Heard, D. E.: Quantifying the magnitude of a missing hydroxyl radical source in a tropical rainforest, Atmos. Chem. Phys. Discuss., 11, 5785–5809, doi:10.5194/acpd-11-5785-2011, 2011. 11316, 11336

Yoshino, A., Sadanaga, Y., Watanabe, K., Kato, S., Miyakawa, Y., Matsumoto, J., and Kajii, Y.: Measurement of total OH reactivity by laser-induced pump and probe technique – comprehensive observations in the urban atmosphere of Tokyo, Atmos. Environ., 40, 7869–7881, 2006. 11315

Zhang, Y. H., Hu, M., Zhong, L. J., Wiedensohler, A., Liu, S. C., Andreae, M. O., Wang, W., and Fan, S. J.: Regional integrated exeriments on air quality over Pearl River Delta 2004 (PRIDE-PRD2004): overview, Atmos. Environ., 42, 6157–6173, 2008. 11317

Zhang, Y. H., Hu, M., Shao, M., Brauers, T., Chang, C. C., Hofzumahaus, A., Holland, F., Li, X., Lu, K., Kita, K., Kondo, Y., Nowak, A., Pöschl, U., Rohrer, F., Zeng, L., Wiedensohler, A., and Wahner, A.: Continuous efforts to investigate regional air pollution in the Pearl River Delta, China: PRiDe PRD2006 campaign, Atmos. Chem. Phys., in preparation, 2011. 11317

Table 1. Instruments for atmospheric trace gas measurements at Backgarden in summer 2006.

Compound	Measurement technique	Time resolution	LOD (1σ)	Accuracy (1σ)
OH	Laser induced fluorescence	5 min	(0.5–1) ×10^6 cm^{-3}	20%
HO_2^* [a]	Chemical conversion and laser induced fluorescene	5 min	(1–3) ×10^6 cm^{-3}	(b)
O_3	UV photometry	1 min	0.3 ppb	5%
NO	Chemiluminescence	1 min	50 ppt	7%
NO_2	Photolytical converter and chemiluminescence	1 min	170 ppt	13%
HONO	LOPAP[c]	5 min	7 ppt	10%
CO	IR photometry	1 min	4 ppb	5%
CH_4	FTIR[d]	10 min	0.5 ppm	4%
C_2H_6	Canister sample – GC[e]	10 s	2 ppt	5%
C_2H_4	Canister sample – GC[e]	10 s	3 ppt	10%
C_3–C_{12} VOCs	Online – GC[e]	1 h	6–70 ppt	10%

[a] HO_2 measurement contains an uncorrected contribution by RO_2.

[b] 20% by calibration plus contribution by RO_2 interference (see text).

[c] Long-path absorption photometry.

[d] Fourier-transform infrared spectrometry.

[e] Gas chromatography; see measured species in Table 2.

Table 2. Measured hydrocarbons and their assignment to RACM species.

RACM	Measured hydrocarbons
CH_4	Methane
ETH	Ethane
HC3	Propane, *n*-Butane, *i*-Butane, 2,2-Dimethylbutane
HC5	*n*-Pentane, *i*-Pentane, Cyclopentane,*n*-Hexane, 2,3-Dimethylbutane, 2-Methylpentane, 3-Methylpentane, *n*-Heptane, 2,4-Dimethylpentane, 2,3-Dimethylpentane
HC8	Cyclohexane, Methylcyclopentane, 2-Methylhexane, 3-Methylhexane, Methylcyclohexane, *n*-Octane, 2-Methylheptane, 3-Methylheptane, *n*-Nonane, *n*-Decane, *n*-Undecane, *n*-Dodecane,
ETE	Ethene
OLT	Propene, 1-Butene, 1-Pentene
OLI	*cis*-2-Butene, *trans*-2-Butene, *cis*-2-Pentene, *trans*-2-Pentene
ISO	Isoprene
TOL	Benzene, Toluene, Ethylbenzene, *n*-Propylbenzene, *i*-Propylbenzene
XYL	*o*-Xylene, *m*-Xylene, *p*-Xylene, *o*-Ethyltoluene, *m*-Ethyltoluene, *p*-Ethyltoluene, Styrene, *m*-Diethylbenzene, *p*-Diethylbenzene, 1,2,3-Trimethylbenzene, 1,2,4-Trimethylbenzene, 1,3,5-Trimethylbenzene

Title Page
Abstract | Introduction
Conclusions | References
Tables | Figures
◀| |▶
◀ ▶
Back | Close
Full Screen / Esc
Printer-friendly Version
Interactive Discussion

Table 3. Mean values of atmospheric parameters measured from 06:00 to 10:00 CNST and 12:00 to 16:00 CNST at Backgarden during 5–25 July 2006, when measured data for OH and k_{OH} were simultaneously available.

Parameter	Mean value	
	06:00–10:00	12:00–16:00
O_3 (ppb)	18	62
NO (ppb)	8.8	0.14
NO_2 (ppb)	16.9	1.4
HONO (ppb)	1.5	0.21
CO (ppb)	1140	420
CH_4 (ppm)[a]	2.5	1.9
Ethane (ppb)[b]	1.5	1.5
Ethene (ppb)[b]	3	3
Isoprene (ppb)	1.0	1.8
HC3 (ppb)[c]	6.8	1.4
HC5 (ppb)[c]	5.3	0.6
HC8 (ppb)[c]	4.0	0.2
OLI (ppb)[c]	0.5	0.07
OLT (ppb)[c]	2.9	0.64
TOL (ppb)[c]	8.3	1.2
XYL (ppb)[c]	2.8	0.16
H_2O (% abs)	3.3	3
k_{OH} (s^{-1})	40.6	17.9
Photolysis frequencies (s^{-1})		
$O_3 \rightarrow O^1D$	0.61×10^{-5}	2.6×10^{-5}
$NO_2 \rightarrow NO + O$	2.9×10^{-3}	6.6×10^{-3}
$HONO \rightarrow NO + OH$	5.3×10^{-4}	1.2×10^{-4}
$HCHO \rightarrow H_2 + CO$	1.14×10^{-5}	2.9×10^{-5}
$HCHO \rightarrow H + HCO$	0.86×10^{-5}	2.5×10^{-5}
Temperature (°C)	29.5	33.6
Pressure (hPa)	1001	998

[a] Fourier transform spectrometer measurements (P. Xie, personal communication).

[b] Fixed value, from gas chromatography measurements of canister samples.

[c] See VOC assignment in Table 2.

Title Page
Abstract | Introduction
Conclusions | References
Tables | Figures
◀I | ▶I
◀ | ▶
Back | Close
Full Screen / Esc
Printer-friendly Version
Interactive Discussion

Table 4. Relative RO_2 detection sensitivities (α_{RO_2}) used for the calculation of modelled HO_2^* concentrations.

Hydrocarbons[a]	RACM Peroxy radicals[b]	α_{RO_2}	Remark
CH_4	MO2	0.04 ± 0.04	exp.[c]
ETH	ETHP	0.07 ± 0.03	exp.[c]
HC3	HC3P	0.07 ± 0.03	estimated (ethane)[d]
HC5	HC5P	0.48 ± 0.18	estimated (cyclohexane)[d]
HC8	HC8P	0.48 ± 0.18	estimated (cyclohexane)[d]
ETE	ETEP	0.85 ± 0.05	exp.[c]
OLT	OLTP	0.95 ± 0.03	estimated (propene)[d]
OLI	OLIP	0.95 ± 0.03	estimated (propene)[d]
ISO	ISOP	0.79 ± 0.05	exp.[c]
MACR/MVK	MACP	0.59 ± 0.07	exp.[c,e]
TOL	TOLP	0.86 ± 0.13	estimated (benzene)[d]
XYL	XYLP	0.86 ± 0.13	estimated (benzene)[d]

[a] See Table 2.

[b] Peroxy radicals formed from the OH+hydrocarbon reaction in 1 atm of air.

[c] Experimental value and 1-σ measurement error from Fig. 3.

[d] Estimated; the experimental value for the hydrocarbon specified in paranthesis has been adopted. The 1-σ error bar includes the experimental error of the specified hydrocarbon and the variability of the calculated $\alpha^i_{RO_2}$ values in the corresponding RACM group, as shown in Fig. 3.

[e] Mean value for MVK and MACR.

Table 5. Chemical mechanisms used in box model simulations of HO_x for PRIDE-PRD2006.

Simulation	Chemical mechanisms[a]
M0	RACM-MIM-GK (base case) mechanism by Karl et al. (2006)
M1	as M0, with generic recycling reactions added as proposed by Hofzumahaus et al. (2009): $RO_2 + X \longrightarrow HO_2$ and $HO_2 + X \longrightarrow OH$
M2	as M0, with a single generic recycling reaction added: $HO_2 + Y \longrightarrow OH$
M3	as M0, with additional OH-forming channels in reactions of acyl peroxy + HO_2 and β-keto peroxy + HO_2 reactions
M4	as M3, with the OH-reforming mechanism by Paulot et al. (2009), in which reactions of OH with isoprene hydroxyhydroperoxides produce epoxides and prompt OH
M5	as M4, with the LIM0 scheme by Peeters and Müller (2010) incorporated, in which isoprene hydroxyperoxy radicals produce prompt HO_2 and HPALDs, followed by HPALDs photolysis. Two variants are tested: a: $\text{HPALDs} + hv \longrightarrow OH + HO_2 + \text{products}$ b: $\text{HPALDs} + hv \longrightarrow 3\,OH + HO_2 + \text{products}$
M6	as M3, with OH-formation from the reaction of isoprene hydroxyperoxy radicals with HO_2 as proposed by Lelieveld et al. (2008) and Butler et al. (2008). Two variants are tested: a: $\text{ISOP} + HO_2 \longrightarrow 2OH + \text{products}$ b: $\text{ISOP} + HO_2 \longrightarrow 4OH + \text{products}$
M7	MCMv3.1(Saunders et al., 2003; Jenkin et al., 2003)

[a] A detailed description and a listing of the mechanisms M0–M6 can be found in the Supplement of this paper.

Table 6. Noontime maxima of measured HO_x concentrations at urban and suburban sites during summer time. All the cited radical measurements were performed by LIF techniques.

Site	Month, year	OH^a (10^6 cm^{-3})	$HO_2{}^{a,b}$ (10^8 cm^{-3})	$j(O^1D)^c$ (10^{-5} s^{-1})	Reference
Los Angeles (34° N)	Sep 1993	5–7	1.4–2	–	George et al. (1999)
Berlin (52.9° N)	Jul–Aug 1998	4–8	2–8	1.5	Holland et al. (2003)
Birmingham (52.4° N)	Jun 1999	2–9	1.5–10	1.5[d]	Emmerson et al. (2005)
Nashville (36.2° N)	Jun–Jul 1999	7.5–20	2.5–20	3[e]	Martinez et al. (2003)
New York City[f] (40.7° N)	Jun–Aug 2001	3–33	0.8–10	2.5	Ren et al. (2003)
Mexico City[f,g] (19.4° N)	Apr 2003	8–13	5–20	3.4[h]	Shirley et al. (2006)
London (51.7° N)	Jul–Aug 2003	1–6	<0.5–2	1–2[a]	Emmerson et al. (2007)
Tokyo (35.6° N)	Jul–Aug 2004	5–13	0.7–14	2.5	Kanaya et al. (2007b)
Houston (29.7° N)	Aug 2000	≈18	≈7	3.0	Mao et al. (2010)
Houston (29.7° N)	Sep 2006	≈14	≈10	3.0	Mao et al. (2010)
Guangzhou (23.5° N)	Jul 2006	15–26	3–25	3.5	This work

[a] Range of reported daily noontime maxima.

[b] Observed HO_2 values by LIF instruments uncorrected for RO_2 interferences (see Sect. 2.3).

[c] Mean noontime value.

[d] Value from a single day (Harrison et al., 2006).

[e] Value from a single day (Thornton et al., 2002).

[f] The radical concentrations in this table is 1.64 times larger than that reported originally according to Mao et al. (2010).

[g] Located at about 2240 m above sea level.

[h] Scaled to be 1.36 higher than in New York City during summer 2001 (Ren et al., 2003) as stated in Shirley et al. (2006).

Table 7. Reaction rates (ppb h^{-1}) and radical parameters averaged over the afternoon hours (12:00–16:00 CNST) from observation (Exp) and different model scenarios (M0–M7).

Reaction rate (ppb h^{-1})	Exp	M0	M1	M2	M3	M4	M5a	M5b	M6a	M6b	M7
OH budget											
$D(OH)=[OH] \times k_{OH}$	34.1	10.4	46.3	40.9	11.0	11.0	15.6	21.8	14.4	21.5	9.7
$k_7[HO_2][NO]$	5.8[a]	5.0	6.4	1.3	5.1	5.2	7.2	8.4	5.6	6.5	4.7
$2k_{13}[O^1D][H_2O]$	2.4	2.4	2.4	2.4	2.4	2.4	2.4	2.4	2.4	2.4	2.3
$j(HONO)[HONO]$	0.9	0.9	0.9	0.9	0.9	0.9	0.9	0.9	0.9	0.9	0.9
$D(OH)-P'(OH)$[b]	25.0[a]	2.1	36.7	36.3	2.6	2.6	5.1	10.1	5.5	11.8	1.8
Additional OH sources											
$HO_2 + X \rightarrow OH$			33.7								
$HO_2 + Y \rightarrow OH$				34.4							
$R(C{=}O)R'O_2 + HO_2 \rightarrow OH$[c]					0.4	0.4	0.5	0.6	0.6	1.0	
$IEPOXO2 + HO_2 \rightarrow OH$[d]						0.1	0.1	0.1			
$ISOP \rightarrow OH$[e]							0.3	0.5			
$HPALDs + hv \rightarrow m \times OH$[e]							1.4	5.1			
$ISOP + HO_2 \rightarrow n \times OH$[f]									2.2	7.1	
Other reactions											
ISOP + NO		0.9	0.9	4.1	0.9	1.0	0.3	0.4	1.1	1.5	1.0
$HCHO + hv \rightarrow 2 \times HO_2$		2.8	5.9	4.4	2.8	2.8	3.1	3.2	3.0	3.2	2.4
$OVOCs + hv \rightarrow HO_2$[g]		0.7	1.6	1.3	0.7	0.7	2.2	2.6	0.8	1.0	0.6
Ozone production											
$P(O_3)$		10.7	11.3	19.9	10.9	10.7	12.5	14.7	12.4	15.1	10.7
$P(O_3)/([OH] \times k_{OH})$		1.0	0.2	0.5	1.0	1.0	0.8	0.7	0.9	0.7	1.1
Radical parameters											
OH (10^6 cm^{-3})	12.6	3.1	12.2	11.8	3.3	3.4	4.8	6.3	4.1	5.6	3.3
k_{OH} (s^{-1})	17.9	21.6	24.9	22.8	21.8	21.3	21.3	22.8	23.0	25.2	21.0
RO_2/HO_2		1.2	0.8	21.4	1.2	1.1	0.7	0.8	1.3	1.5	1.2
HO_2/OH	< 136[a]	362	125	23	351	345	343	303	311	263	345

[a] Based on uncorrected HO_2^* values ($[HO_2^*] > HO_2$).

[b] $P'(OH) = 2k_{13}[O^1D][H_2O] + j(HONO)[HONO] + k_7[HO_2][NO]$.

[c] R′ = H or CH_2, according to Taraborrelli et al. (2009).

[d] According to Paulot et al. (2009).

[e] According to Peeters and Müller (2010).

[f] According to Lelieveld et al. (2008).

[g] OVOCs without HCHO.

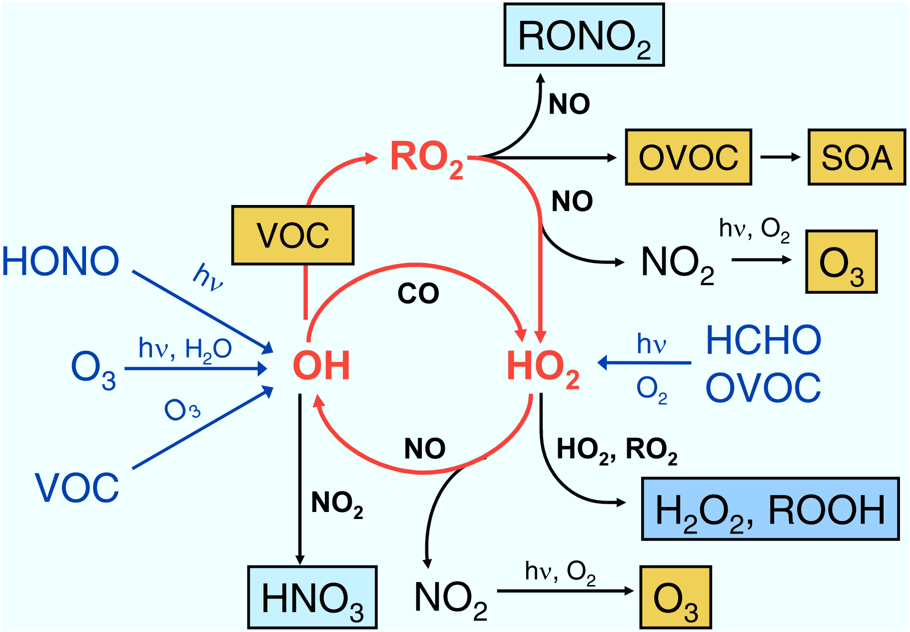

Fig. 1. Schematic drawing of HO_X chemistry, illustrating established, major chemical pathways in the troposphere. Radical chemistry is initiated by primary radical production (blue arrows) through photodissociation and ozonolysis reactions and is terminated by radical recombination reactions forming nitric acid (HNO_3), hydroperoxides (H_2O_2, ROOH) and organic nitrates ($RONO_2$). Radical chain reactions (red arrows) cause cycling between OH, HO_2, and RO_2. Reactions of RO_2 and HO_2 with NO reproduce OH (secondary OH production) and lead to photochemical formation of ozone, OVOCs and SOA.

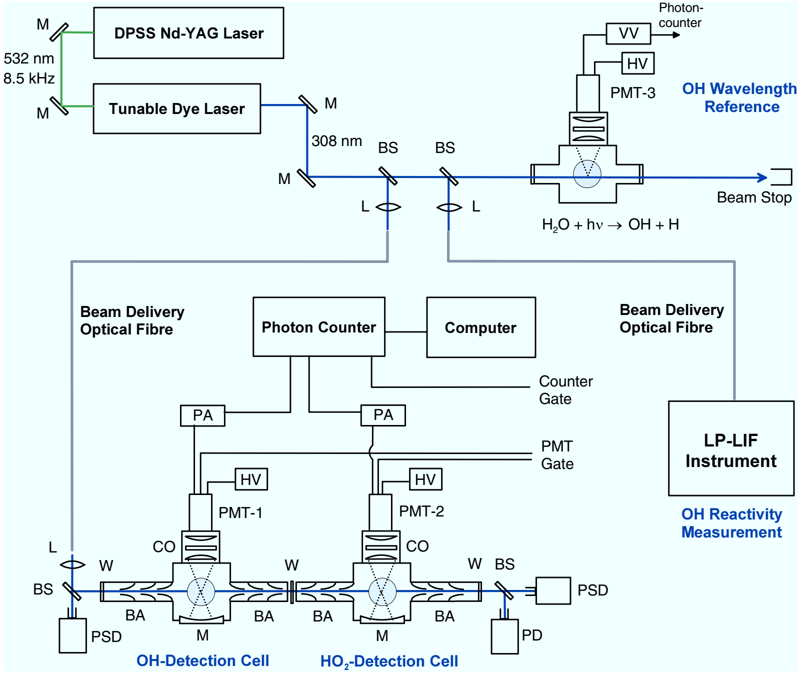

Fig. 2. Schematic drawing of the LIF system. Laser radiation (308 nm) from a tunable dye laser is distributed by beam steering optics (M, BS, L) and optical fibres to **(a)** a pair of independent detection chambers for measurement of OH and HO_2 concentrations, **(b)** a laser photolysis laser-induced fluorescence (LP-LIF) instrument for measurement of k_{OH}, and **(c)** a wavelength reference cell in which photolytically generated OH is monitored by LIF. Note that the sampled ambient air is flowing through the low-pressure detection chambers perpendicular to the optical plane shown in the figure. Abbrev.: M mirror, BS beam splitter, L lens, W quartz window, CO fluorescence collection optics, BA laser baffle arm, PD photodiode, PSD position-sensitive photodiode, PMT photomultiplier tube, HV high voltage supply, PA preamplifier.

ACPD
11, 11311–11378, 2011

Title Page
Abstract
Introduction
Conclusions
References
Tables
Figures
◀▮
▶▮
◀
▶
Back
Close
Full Screen / Esc
Printer-friendly Version
Interactive Discussion

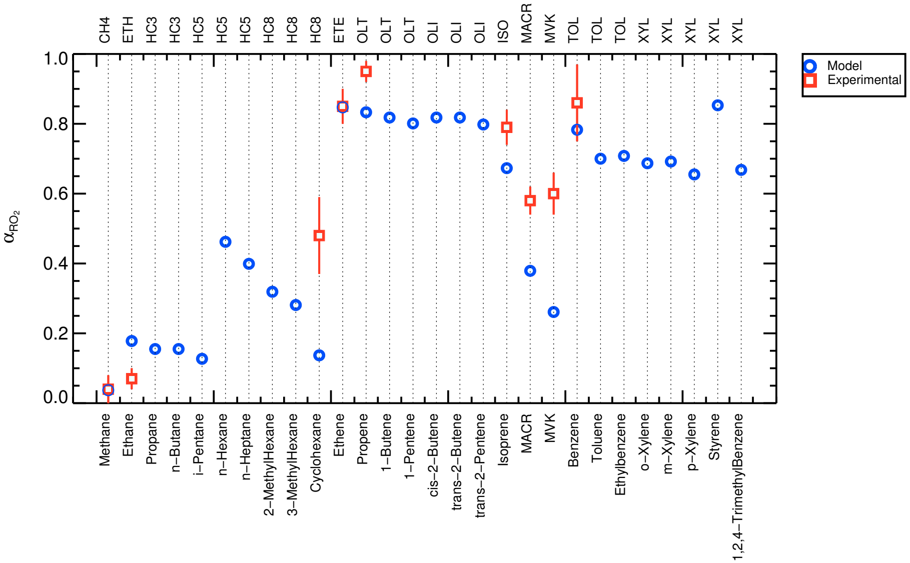

Fig. 3. Relative detection sensitivities ($\alpha^i_{RO_2}$) for specific RO_2 compared to HO_2. The experimental values (red squares) and their 1-σ error bars were determined for the instrument configuration applied at PRD for HO_2 detection (Fuchs et al., 2011). Modelled values are shown for major VOCs which contributed more than 90% to the organic OH reactivity (without HCHO). Original and mechanistic names of the VOCs are shown at the lower and upper x-axis, respectively.

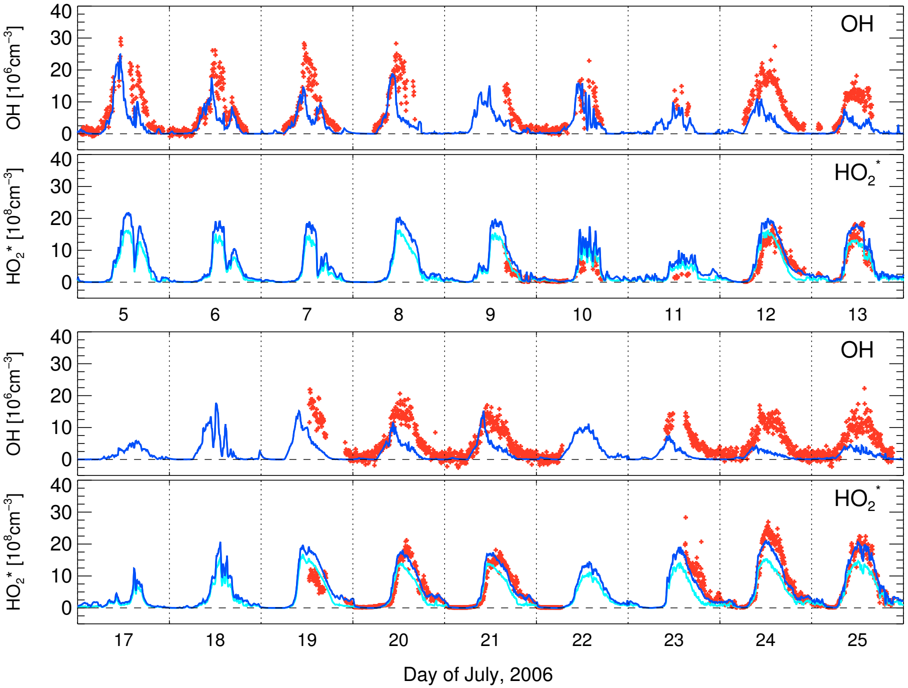

Fig. 4. Time series of 5 min-averaged measured and simulated (M0) concentrations of OH and HO_2^* at the Backgarden site during PRIDE-PRD2006 campaign. Experimental values are denoted by red symbols, modelled values by blue lines. Modelled values of HO_2 are represented by cyan lines. The difference between the lines for HO_2 and HO_2^* is the interference by RO_2 calculated by the base model (RACM-MIM-GK). Vertical dotted lines denote midnight.

Title Page
Abstract | Introduction
Conclusions | References
Tables | Figures
◀| |▶
◀ ▶
Back | Close
Full Screen / Esc
Printer-friendly Version
Interactive Discussion

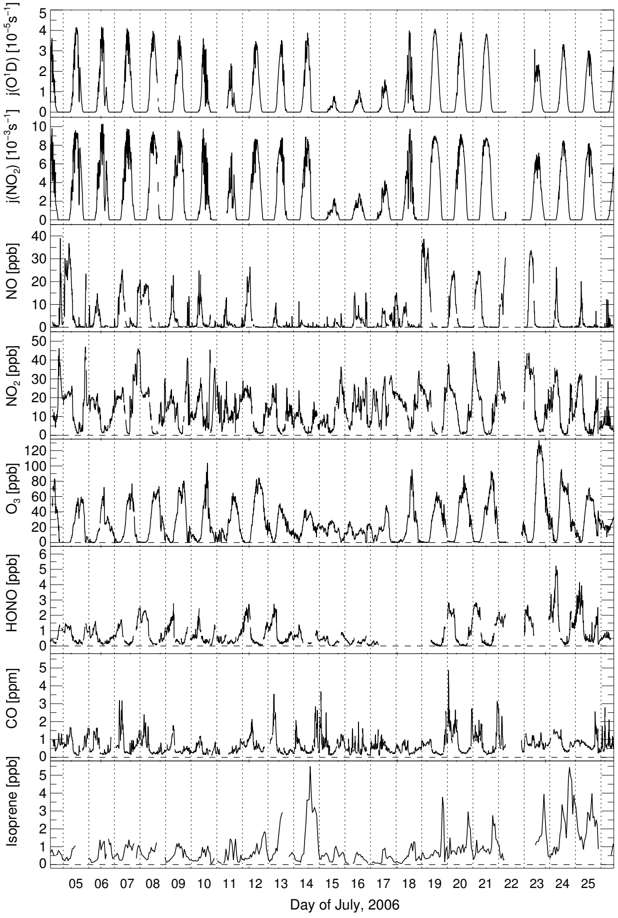

Fig. 5. Time-series of measured $j(O^1D)$, $j(NO_2)$, NO, NO_2, O_3, HONO, CO and isoprene at PRD Backgarden from 5 July to 25 July 2006. Vertical lines denote midnight.

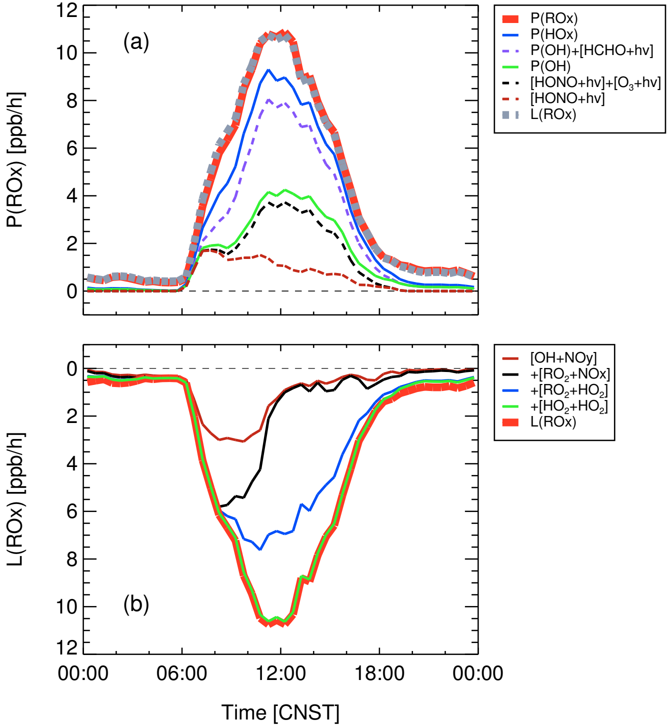

Fig. 6. Production **(a)** and loss rates **(b)** of RO_X radicals (= $OH + HO_2 + RO_2$) calculated with RACM-MIM-GK (M0). Panel **(a)**: breakdown of the primary RO_X production resulting from photolytic processes and ozonolysis. $P(OH)$, $P(HO_X)$, and $P(RO_X)$ denote total, primary production rates of OH, HO_X, and RO_X, respectively. Panel **(b)**: beakdown of the RO_X loss caused by radical termination reactions. The brown solid line denotes the loss rate by $OH + NO_y$, the black solid line by $OH + NO_y$ and $RO_2 + NO_x$, etc. The total RO_X loss rate is given by $L(RO_X)$ which is equal to $P(RO_X)$ shown in panel **(a)**. Legends: the expressions embedded in square brackets represent the corresponding chemical conversion rates.

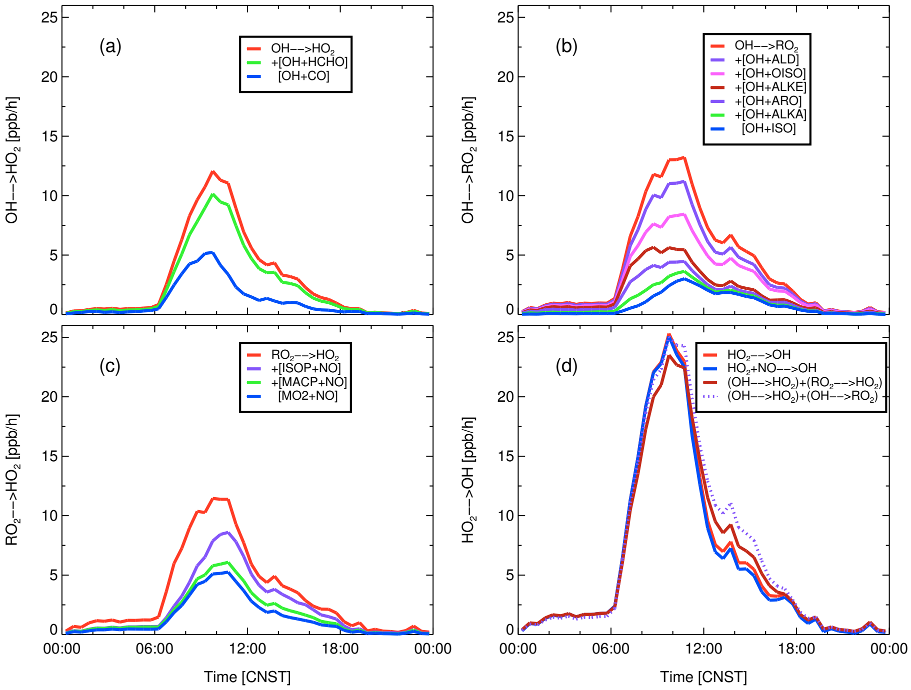

Fig. 7. Radical conversion rates (–) of **(a)** OH → HO$_2$, **(b)** OH → RO$_2$, **(c)** RO$_2$ → HO$_2$, and **(d)** HO$_2$ → OH, calculated with RACM-MIM-GK (M0). The cumulative contributions of dominating reactions are presented as explained in Fig. 6. Panel **(d)**: total OH loss and total HO$_2$ production, both confined to radical conversion reactions, are displayed by the dotted violet and solid brown lines, respectively.

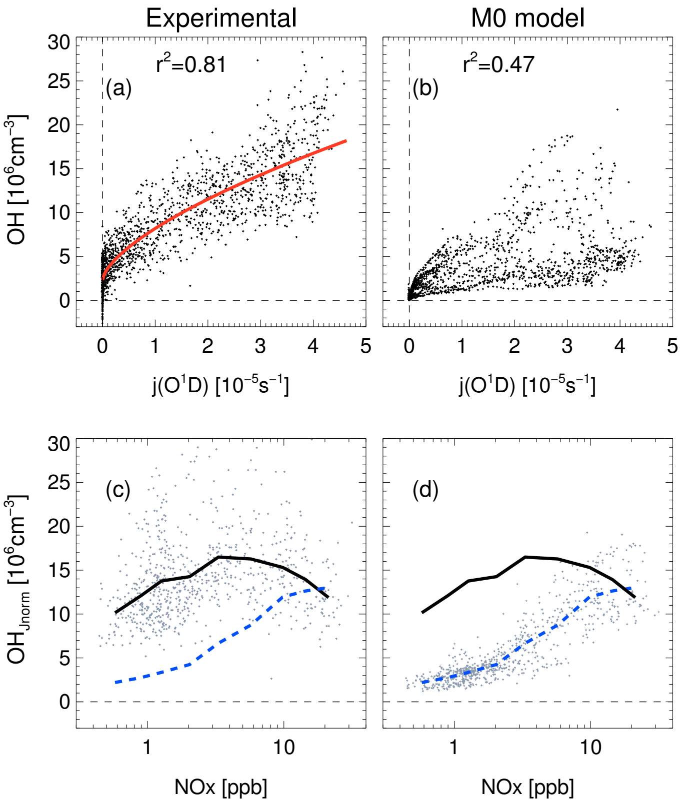

Fig. 8. Correlation of OH with $j(O^1D)$ and NO_x at PRD backgarden. The left panels **(a, c)** show dependencies for measured OH, the right panels **(b, d)** for modelled OH (M0). In panel **(a)**, a Levenberg-Marquard fit to Eq. (2) is shown as red line. In panels **(c)** and **(d)**, the OH data were first selected by $j(O^1D) > 1 \times 10^{-5}\ s^{-1}$, and then normalized to $j(O^1D)$ (see text), denoted as OH_{Jnorm}. The black solid and the blue dashed lines give the averaged values of measured and modelled OH_{Jnorm}, respectively, over equally spaced $\ln([NO_X]/ppb)$ intervals.

Title Page
Abstract Introduction
Conclusions References
Tables Figures
◀I ▶I
◀ ▶
Back Close
Full Screen / Esc
Printer-friendly Version
Interactive Discussion

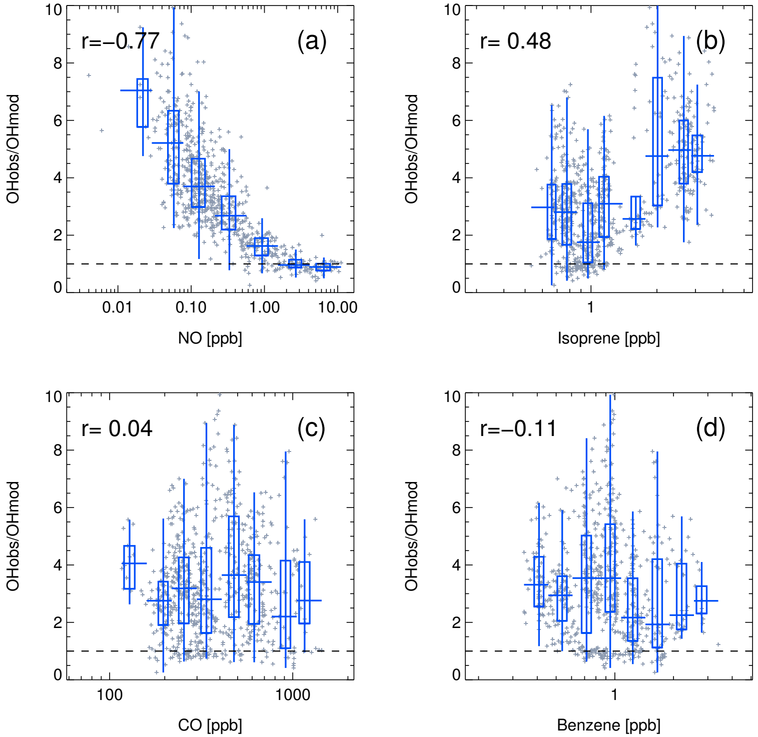

Fig. 9. Measured-to-modelled OH ratios, OH_{obs}/OH_{mod}, plotted versus the mixing ratios of **(a)** NO, **(b)** isoprene, **(c)** CO, and **(d)** benzene. The data have been filtered for $j(O^1D) \geq 1 \times 10^{-5}\ s^{-1}$ and are presented as individual data points (crosses) and in box-and-whisker style (the bottom and top of the boxes mark the lower and upper quartiles, respectively), horizontal lines denote median values, and the lower and upper whiskers the minimum and maximum values, respectively. Correlation coefficients, r, between OH_{obs}/OH_{mod} and the logarithmic values of NO, isoprene, CO and benzene are shown in corresponding panels as well.

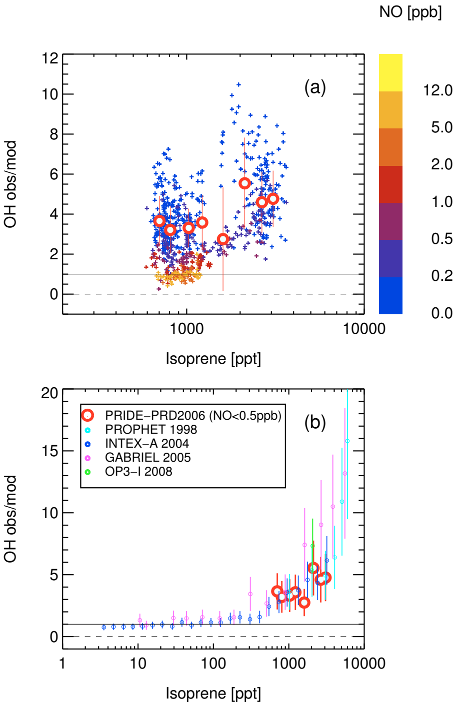

Fig. 10. The observed-to-modelled OH ratio as a function of isoprene at PRD backgarden **(a)** and its comparison to ratios reported from other field campaigns **(b)**. Panel **(a)**: the individual data points from Fig. 9b are color coded according to concurrently measured NO mixing ratios. The red open circles are average values of OH_{obs}/OH_{mod} over equally spaced ln([isoprene]/ppb) intervals for NO lower than 0.5 ppb. The error bars denote the variability within each NO interval. Panel **(b)**: the averaged values from panel **(a)** (red open circles) are compared to OH_{obs}/OH_{mod} ratios reported from PROPHET (1998), INTEX (2004), GABRIEL (2006), and OP3-I (2008). Here, the error bars denote the stated measurement accuracies (2σ) of OH.

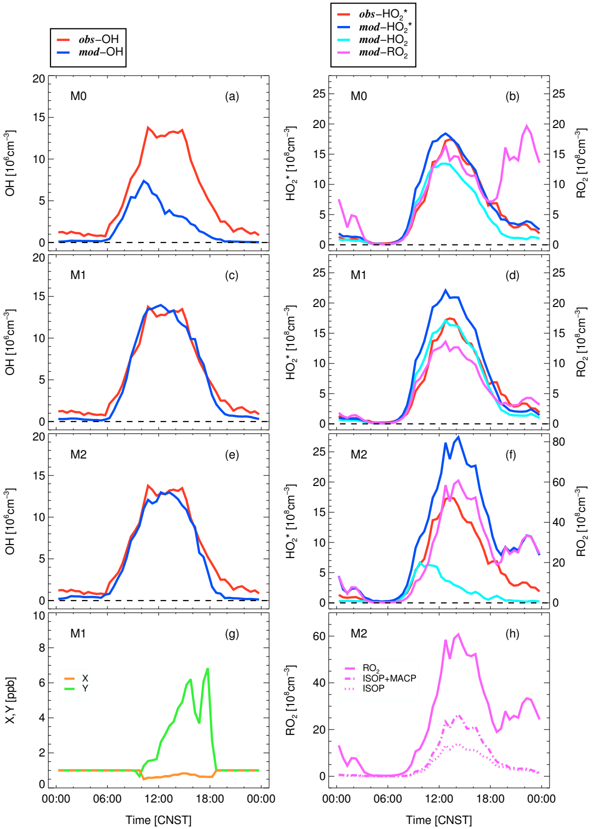

Fig. 11. Comparison of measured and modelled concentrations of OH and HO_2^* for three mechanistic scenarios (M0, M1 and M2). Panels **(b)**, **(d)** and **(f)** show the modelled values of HO_2 and RO_2 as well. The fitted concentrations of the generic species X (scenario M1) and Y (scenario M2) are presented as NO equivalents in panel **(g)**, and model results for peroxy radicals (ISOP, ISOP+MACP, total RO_2) in panel **(h)**.

ACPD
11, 11311–11378, 2011

Title Page
Abstract | Introduction
Conclusions | References
Tables | Figures
◀| |▶
◀ ▶
Back | Close
Full Screen / Esc
Printer-friendly Version
Interactive Discussion

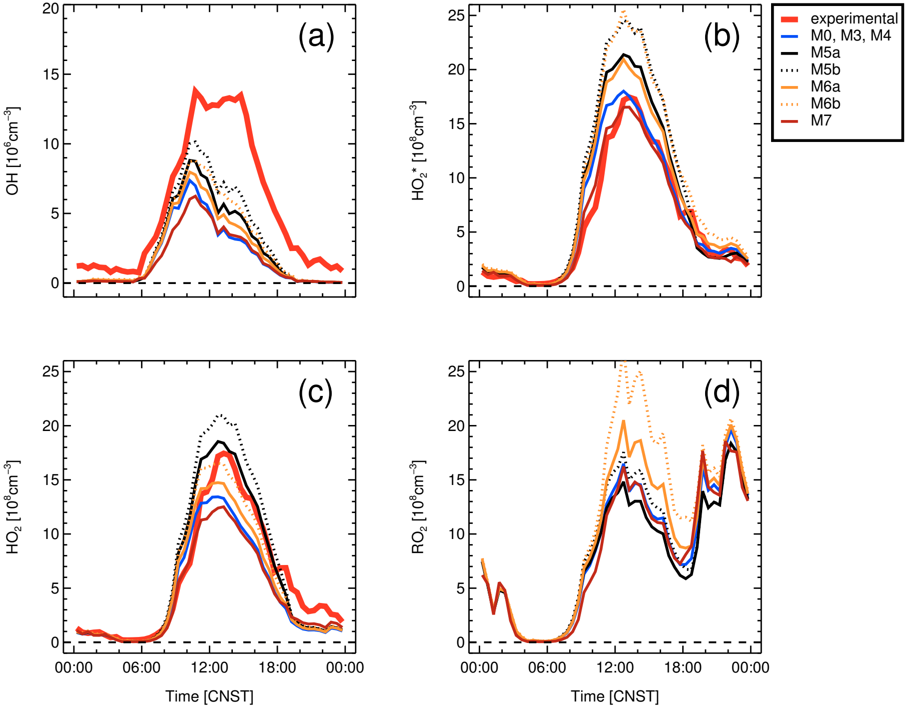

Fig. 12. Comparison of measured and modelled concentrations of OH **(a)** and HO$_2^*$ **(b)**, HO$_2$ **(c)**, and RO$_2$ **(d)** for six different mechanistic scenarios: M0, M3, M4, M5a, M5b, M6, M7. The results for each radical species are not distinguishable among the model runs M0, M3 and M4 (differences are within the thickness of the lines).

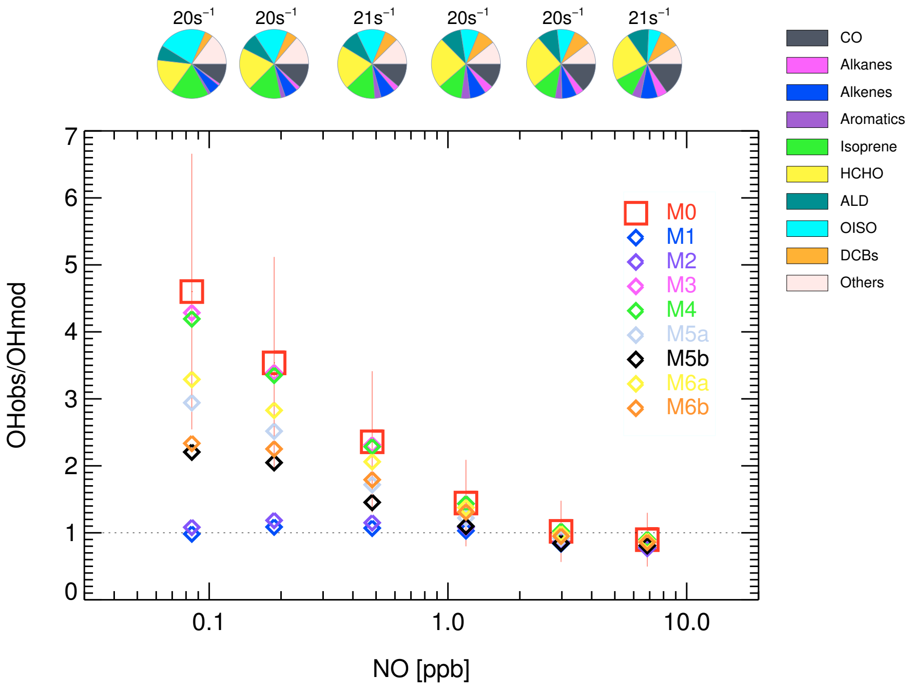

Fig. 13. NO dependence of the observed-to-modelled OH ratio (OH_{obs}/OH_{mod}) for the different mechanistic scenarios M0 to M6 (see Table 5). Vertical error bars denote the combined 1σ accuracies of the modelled (M0) and observed OH concentrations. Total VOC reactivities (M0 case) and their speciation (pie charts) are presented at different NO intervals ($\Delta\ln([NO]/ppb) = 0.17$) at the top. Abbrev. in the color legend of the pie charts: ALD = higher aldehydes than HCHO, OISO = MACR + MVK + CAR4, DCBs = MGLY + GLY + DCB, others = degradation products from hydrocarbons listed in Table 2 that exclude HCHO, ALD, OISO, DCBs .